ORIGINAL RESEARCH ARTICLE

Implementation of Machine Learning Algorithms for Weld Quality Prediction and Optimization in Resistance Spot Welding

Nevan Nicholas Johnson [ID], Vaishnav Madhavadas [ID], Brajesh Asati [ID], Anoj Giri [ID], Shinde Ajit Hanumant [ID], Nikhil Shajan [ID], Kanwer Singh Arora [ID], and Senthil Kumaran Selvaraj [ID]

The manufacturing industry constantly aims to improve product quality while improving production speed and lowering production costs. Resistance spot welding (RSW) is widely used in the automotive industry to join thin sheets of coated and uncoated materials. Manufacturers measure weld quality by performing destructive tests like peel and with the help of metallographic examination, which is time-consuming. Further, critical welding parameters need to be optimized to achieve consistent and predictable weld quality. This work addresses the effects of the three critical welding parameters: welding current, welding time, and electrode force on RSW of 1.40-mm-thick DP780 steel sheets. The weld quality indicators studied are nugget diameter (from the peel test), peel strength, tensile shear strength, and the mean dynamic contact resistance. Artificial neural network and adaptive neuro-fuzzy inference system models were used to predict the weld quality indexes, and the prediction accuracy was found to be 99.36 and 99.98%, respectively. A mathematical model was developed using regression analysis to correlate the welding parameters and weld quality indicators. The multi-objective optimization of the welding parameters was done using the genetic algorithm, and its results were validated experimentally. It was found that the welding current had the most significant impact on the weld quality, followed by the electrode force and the welding time.

1. Introduction

Resistance spot welding (RSW) is a solid-state welding technique used for the joining of two faying surfaces (mostly sheet metals) by the application of pressure and the heat produced by the workpieces' resistance to the passage of electrical current (Ref 1, 2). Pressure is applied via the electrodes to ensure sufficient contact between the two workpieces. Generally, copper alloy electrodes are designed to supply the necessary current density and pressure at the weld location (Ref 3). The temperature rises at the sheet–sheet interface due to resistance heating (Ref 4). When the temperature at the sheet–sheet interface reaches its melting point, they start to fuse, forming an autogenous weld called a nugget (Ref 5, 6). The weld nugget is then allowed to cool and solidify under pressure by water-cooled electrodes, which can dissipate heat by conduction after the current is turned off (Ref 7). RSW

Nevan Nicholas Johnson, Vaishnav Madhavadas, Anoj Giri, and Senthil Kumaran Selvaraj, School of Mechanical Engineering, Vellore Institute of Technology, Vellore 632014, India; and Brajesh Asati, Shinde Ajit Hanumant, Nikhil Shajan, and Kanwer Singh Arora, Research and Development, TATA Steel Ltd., Jamshedpur 831001, India. Contact e-mail: anoj.giri@vit.ac.in.

parameters need to be optimized to achieve high-quality welds. Welding current (WC), electrode force (EF), and welding time (WT) are the three most essential parameters in RSW (Ref 8, 9). The heat generated depends upon the electric resistance, the thermal conductivity of the two workpieces, and the current passing through the electrodes. The amount of heat generated can be expressed in an equation as follows:

$$Q = \eta \cdot \int_{0}^{t} I^2(t) \cdot R(t) \cdot dt \qquad \text{(Eq 1)}$$

where Q = heat generated (Joules), η = welding thermal efficiency, I = current flowing through electrodes (Amperes), R = resistance offered by workpiece (Ohms), and t = welding time (s).

The physical and metallurgical properties of the workpiece materials and the welding parameters interact intricately during RSW (Ref 10). Previously, optimization of the RSW process was primarily based on known empirical criteria such as weld strength, nugget size, and electrode life. This approach involved conducting experiments to determine the optimal welding conditions based on these criteria. This method was time-consuming and costly to conduct multiple experiments to optimize the RSW process for multiple criteria (Ref 11). Although they have been successfully utilized for many years, it is necessary to fully understand and have better knowledge about the factors that would affect weld nugget formation and growth to benefit from advancements in process design and management (Ref 12, 13). Implementing artificial intelligence (AI) and machine learning (ML) would lead to a greater understanding of weld parameters and their effects on weld

Table 1 Chemical composition of DP780 steel (wt.%)

Fe	C	Mn	P	S	Al	Si	Mo	Ti	N	B
Base	0.078	1.84	0.016	0.002	0.04	0.428	0.22	0.02	0.0048	0.0017

Table 2 Mechanical properties of DP780 steel

| Yield strength, MPa	Ultimate tensile strength, MPa	Uniform elongation, %	Elongation, %	Yield ratio	n-value	R-value
473.3	824	12.96	21.2	0.57	0.139	0.883
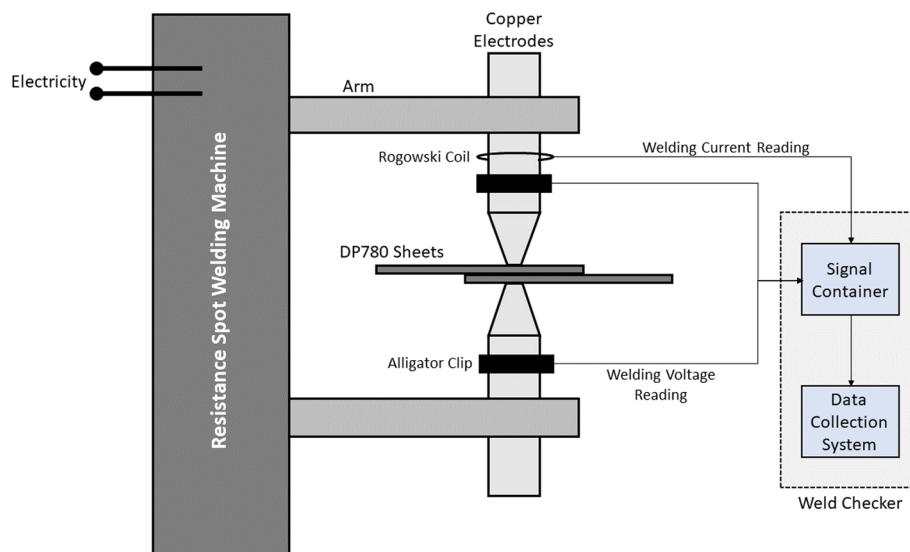
Fig. 1 Schematic of the RSW experimental setup

quality. This would help maximize manufacturing efficiency and minimize defects (Ref 14, 15).

Nowadays, AI and ML have been used widely due to technological advancements and digitalization aimed at improving productivity and eliminating defects. AI and ML are used to automate, make predictions of outcomes, and optimize the manufacturing process (Ref 16, 17). The advantage of using ML in manufacturing is handling multivariate and high-dimensional data to improve quality control optimization and constantly improve complex processes (Ref 18-20). The ML prediction models, if appropriately implemented, will help reduce economic loss and improve productivity (Ref 21).

Nomura et al. used a convolutional neural network model to estimate the weld quality using the molten pool image obtained for the single bevel groove metal active gas welding (Ref 22). The model's prediction accuracy for the burn-through and penetration depth in metal active gas welding was improved when they were considered a regression problem instead of a discontinuous phenomenon. This can be attributed to the regression model's nuanced understanding of the complex relationship between the target and input parameters, enabling it to make predictions for unseen data. By treating the problem as regression, the continuous nature of the target variable is retained, enabling the model to capture and preserve a broader range of information. Unlike discrete classes, a regression model can learn and predict a broad spectrum of values, facilitating a more comprehensive understanding of the problem. The error was less than 1 mm for more than 95% of the sample test cases and less than 0.5 mm for more than 87% of the sample test cases. Further, the image size did not affect the estimation accuracy. Real-time monitoring of the tool was possible as the calculation time was sufficiently short.
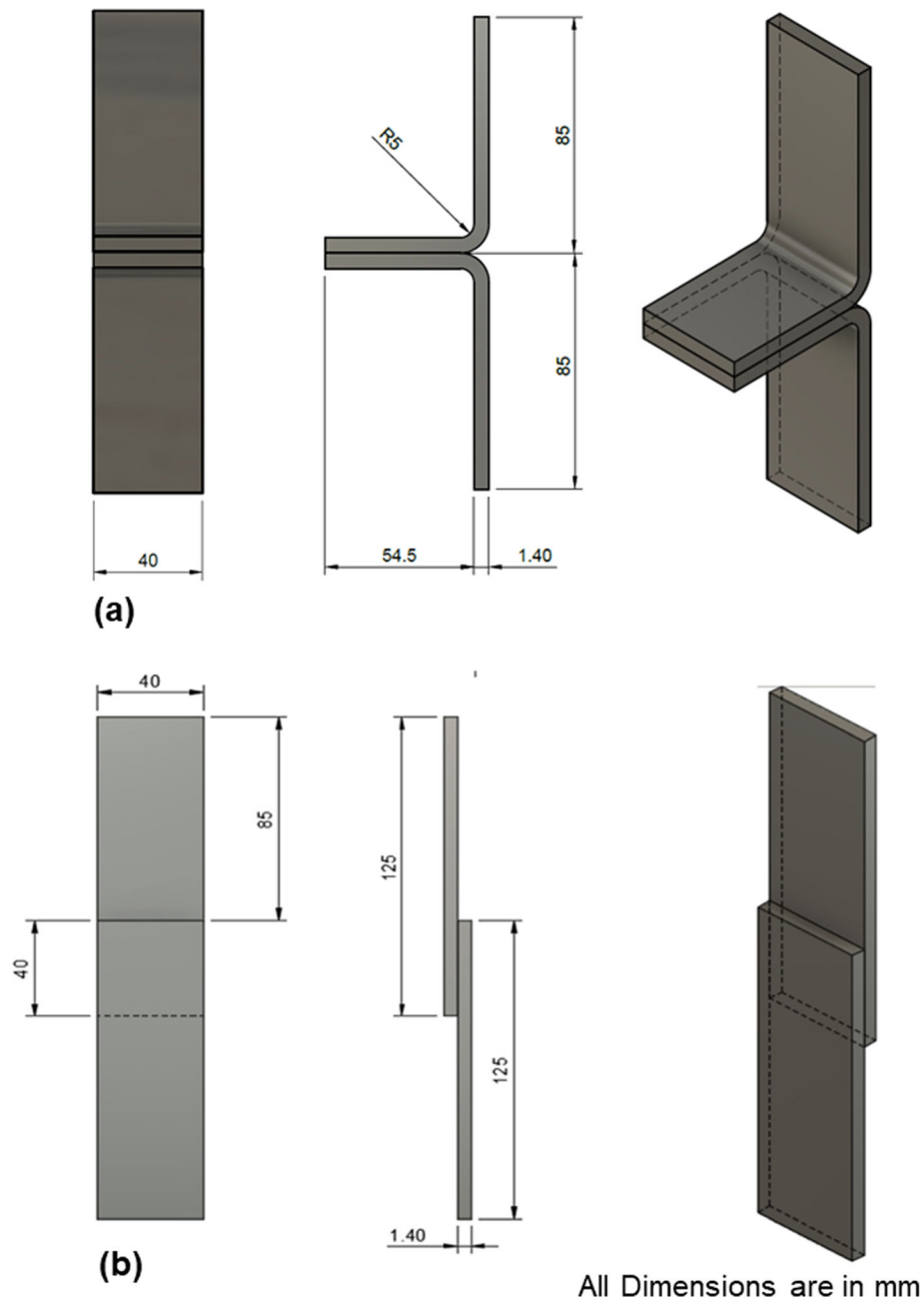
Fig. 2 Dimensions of the weld specimen for (a) coach peel test and (b) tensile shear test

Table 3   Constant welding parameters

Electrode face diameter	Shank diameter	Squeeze time	Hold time	Electrode coolant flow rate
8 mm	16 mm	300 ms	167 ms	4 l/min

Table 4 Critical welding parameters and their factor levels

Sl. No.	Welding parameters	Units	Level 1	Level 2	Level 3	Level 4
1.	WC	kA	5	6	7	8
2.	WT	ms	350	375	400	425
3.	EF	kN	4.15	4.40	4.65	4.90
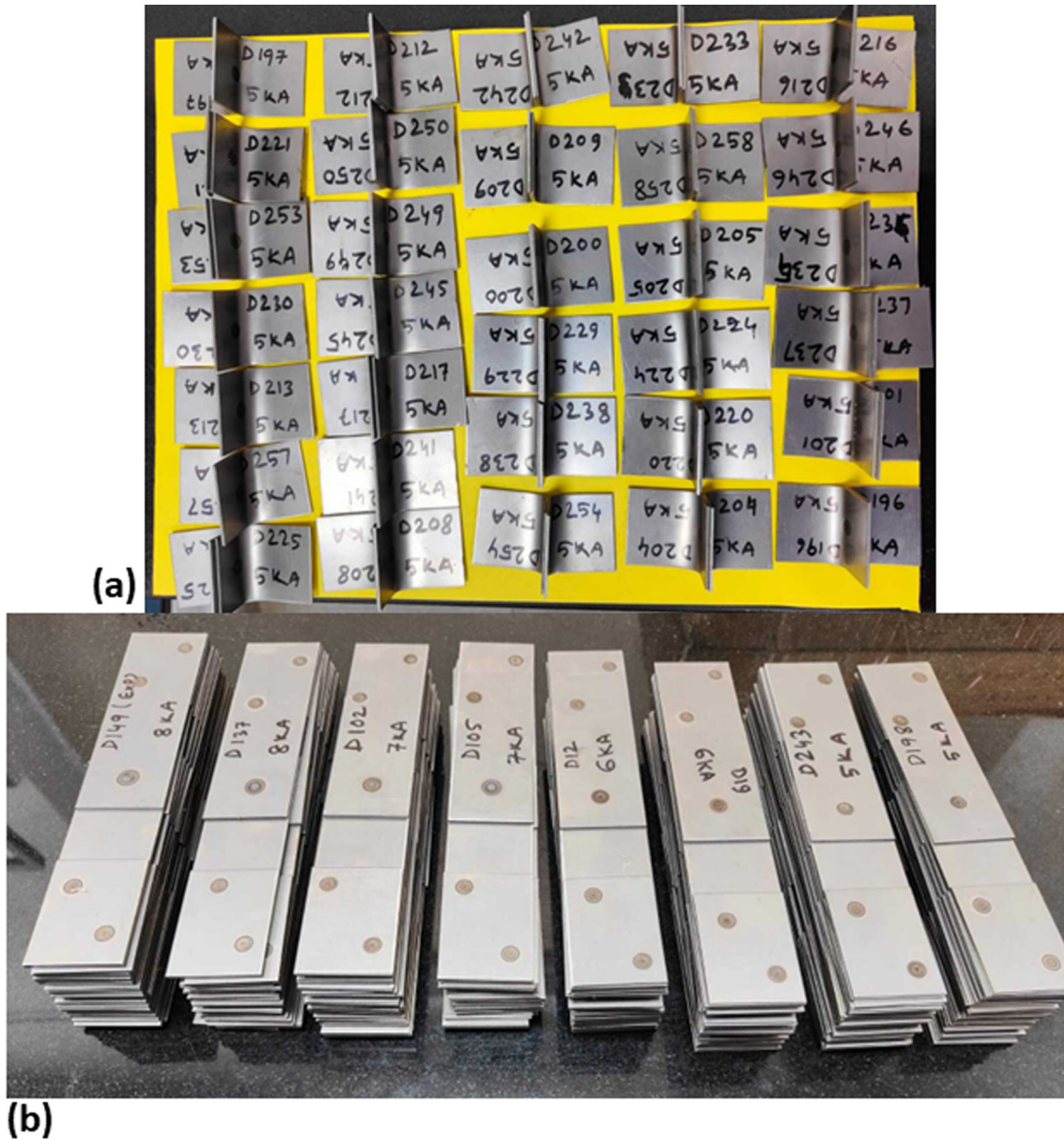
**Fig. 3** Weld samples: (a) coach peel test, (b) tensile shear test
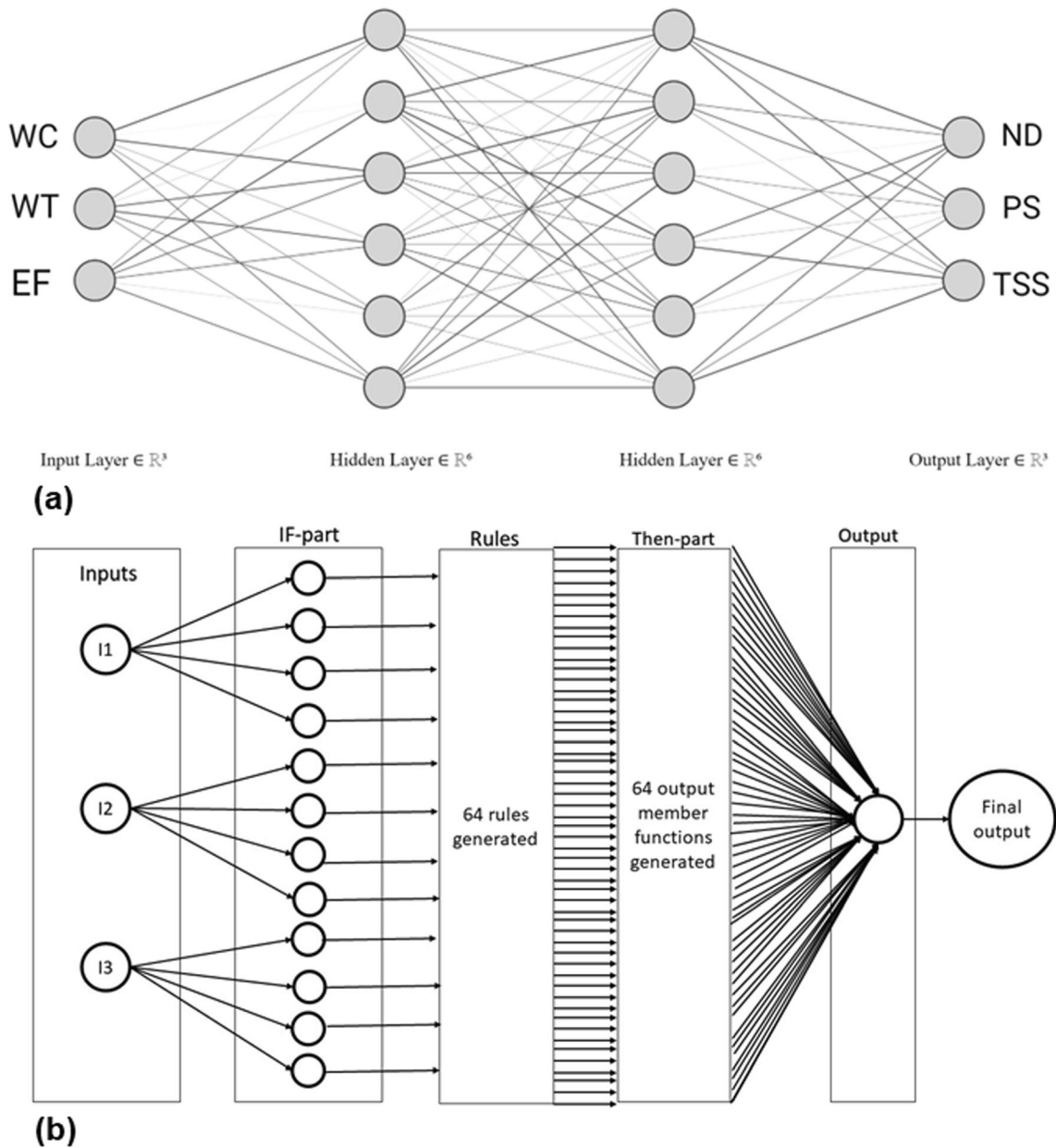
Fig. 4 (a) ANN model architecture, (b) ANFIS model architecture

Mayr et al. found that some of the main challenges in implementing ML are the availability of high-quality data (Ref 23). The ML model's prediction accuracy depends on the training data used. Due to this, if there is any error in the training data, then the ML model's prediction accuracy decreases. The ANN model is a black box model where it is difficult to understand how the algorithm reached the decision.

Due to this, making changes or justifying the model's behavior is challenging. (Ref 24, 25). A viable solution to this problem is using deep fuzzy learning, a combination of fuzzy logic and deep neural network. This hybridization makes the ML algorithm accurate and easily interpreted by humans (Ref 26).

The relationship between the input welding parameters and output weld quality indicators cannot be established linearly
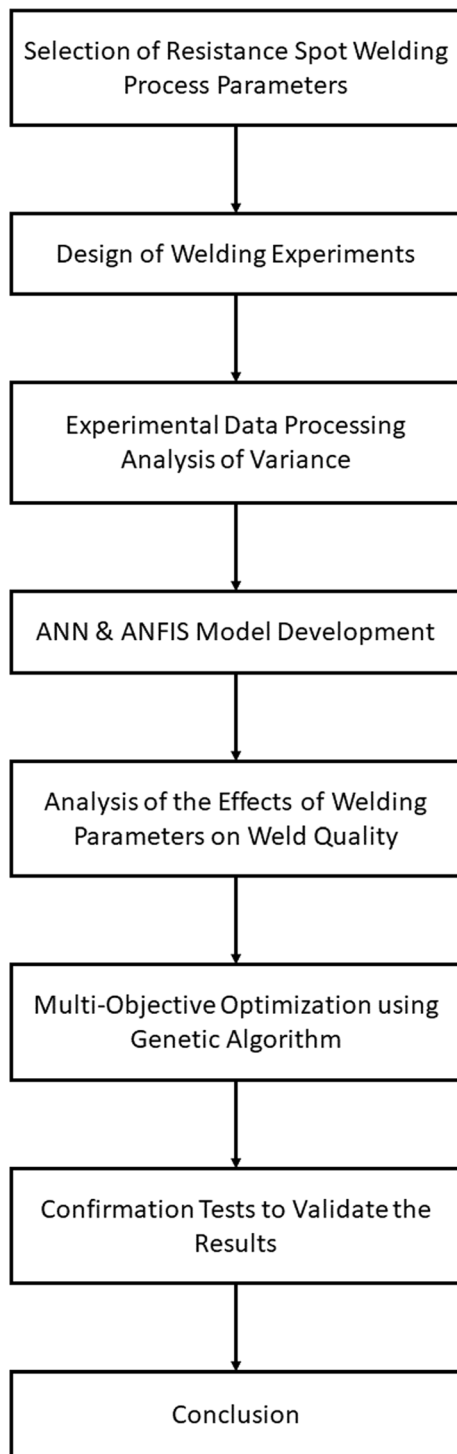
Fig. 5 RSW process parameter optimization procedure

(Ref [27]-[30]). Therefore, it is tough to use mathematical models for accurate prediction. The genetic algorithm (GA) with the least square support vector (GA-LSSVM) can accurately determine the relationship and optimize the process. The GA-LSSVM algorithm predicted the weld quality with 90.6% accuracy (Ref [31]). The precision of the weld quality is limited to the equipment used for the prediction and subjected to human error (Ref [32]). Hwang et al. performed RSW and used adaptive resonance theory artificial neural networks (ART-ANN) in which the input parameters used were welding voltage and current signal (Ref [33]). It was found that the nugget size and the tensile strength were predicted with high accuracy, and the fracture mode was predicted with 100% accuracy. Kitano et al. used the least squares assisted rule extraction from facts, version 5 (LSRF5) method, to derive the equation for the correlation between the input and output parameters (Ref [25]). It is found that the LSRF5 method can be used to predict the nugget diameter (ND).

The cited studies show that GA has extensively optimized complex manufacturing processes. ANN is a very reliable and popular method implemented by most researchers for predicting specific responses in different welding processes. However, there is a remarkable gap in the literature where multiple different ML algorithms are used with multi-objective optimization to find the best algorithm that generalizes the RSW process. The present study aims to implement ML prediction models such as ANN and ANFIS and then compare them to find the most suitable ML model that can accurately predict the RSW weld quality indicators. Further, multi-objective optimization using GA is done to optimize the complex RSW process and generate a set of optimized welding parameters.

2. Methodology

2.1 Material Selection and Experimental Setup

Dual-phase (DP) steel is used extensively in the automotive industry owing to its favorable characteristics, such as high ductility, high strength, low yield-to-tensile ratio, and continuous yielding (Ref [34]). DP780 steel is used in the roof rails, rear rails, body side inner panels, and shock reinforcements of an automobile (Ref [35]). The usage of DP780 is increasing many folds in developing countries such as India as lightweight initiatives and safety concerns are of paramount importance; hence, this paper aims at optimizing the RSW welding parameters for DP780 steel sheets of thickness 1.40 ± 0.05 mm. The chemical composition and mechanical properties of DP780 steel used for the experimentation are listed in Tables 1 and 2, respectively. The mechanical properties were obtained using standard testing procedures and equipment.

Table 5 ANOVA of the multivariate regression model

Sl. No.	Objectives	df	Sum of squares	Mean square	F-value	p-value	R^2-value Adj.	R^2-value Pred.	Model significance
1.	ND	9	104.58	11.62	175.73	1.05×10^{-36}	0.961	0.967	Significant
2.	PS	9	16.37	1.82	12.99	3.82×10^{-10}	0.646	0.701	Significant
3.	TSS	9	1745.38	193.93	252.32	8.17×10^{-41}	0.973	0.977	Significant
4.	MDCR	9	31975.47	3552.83	272.84	1.04×10^{-41}	0.975	0.978	Significant

Table 6 Aim and weightage of objectives

Sl. No.	Objectives	Aim	Weightage
1.	ND	Maximize	*****
2.	TSS	Maximize	****
3.	PS	Maximize	***
4.	MDCR	Minimize	*

Table 7 Genetic algorithm parameters

Sl. No.	Algorithm parameter	Set value
1.	Population size	85
2.	Maximum number of generations	500
3.	Maximum stall generations	200
4.	Selection function	Stochastic uniform
5.	Crossover function	Scattered
6.	Crossover fraction	0.8
7.	Mutation function	Gaussian

The RSW experimentation to generate the weld data was carried out on a pedestal-type 150 kVA medium-frequency direct current machine. The electrodes were made of a copper–chromium–zirconium alloy with a truncated cone shape, a face diameter of 8 mm, and a shaft diameter of 16 mm. The WC and voltage were recorded using a weld checker at an interval of 1 ms. Alligator clips were fastened to the electrodes to measure the voltage, and a Rogowski coil was used to measure the WC. The experimental setup is depicted in Fig. 1. A weld nugget growth curve was also generated. The dimensions of the weld samples for the coach peel and tensile shear tests are shown in Fig. 2. The weld sample in Fig. 2(b) is converted into the coach peel test geometry (T shape) to determine the peel strength (PS).

2.2 Design of Experiment

The experimentation was performed as per a four-level full factorial design. This was achieved by varying three critical input welding parameters in 4 levels of intensity to ensure the completion of different combinations of the welding parameters with a minimum number of experimental runs. This work considers the three critical welding parameters: WC, WT, and EF. The other less significant welding parameters, such as squeeze time, hold time, and coolant flow rate, were kept constant, and their values are shown in Table 3. Trail experiments were done to determine the feasible range of process parameters that could be used such that there was minimum expulsion. Table 4 shows the design of the experiment and the ranges of the critical welding parameters.

The weld quality was assessed based on four indicators: ND, PS, tensile shear strength (TSS), and mean dynamic contact resistance (MDCR). A total of 256 samples were prepared to ascertain the weld quality. The MDCR was calculated from the WC, and voltage data that were recorded using a weld checker during the experimental runs. The welded specimens used for the coach peel test and tensile shear test are shown in Fig. 3. Tensile shear and coach peel tests were performed using the universal testing machine following the JIS Z3136 and JIS Z3144 standards, respectively. During the coach peel test, the peel angle was 90° and the crosshead velocity (peel rate) was set to 5 mm/min. The ND measurements were taken using a
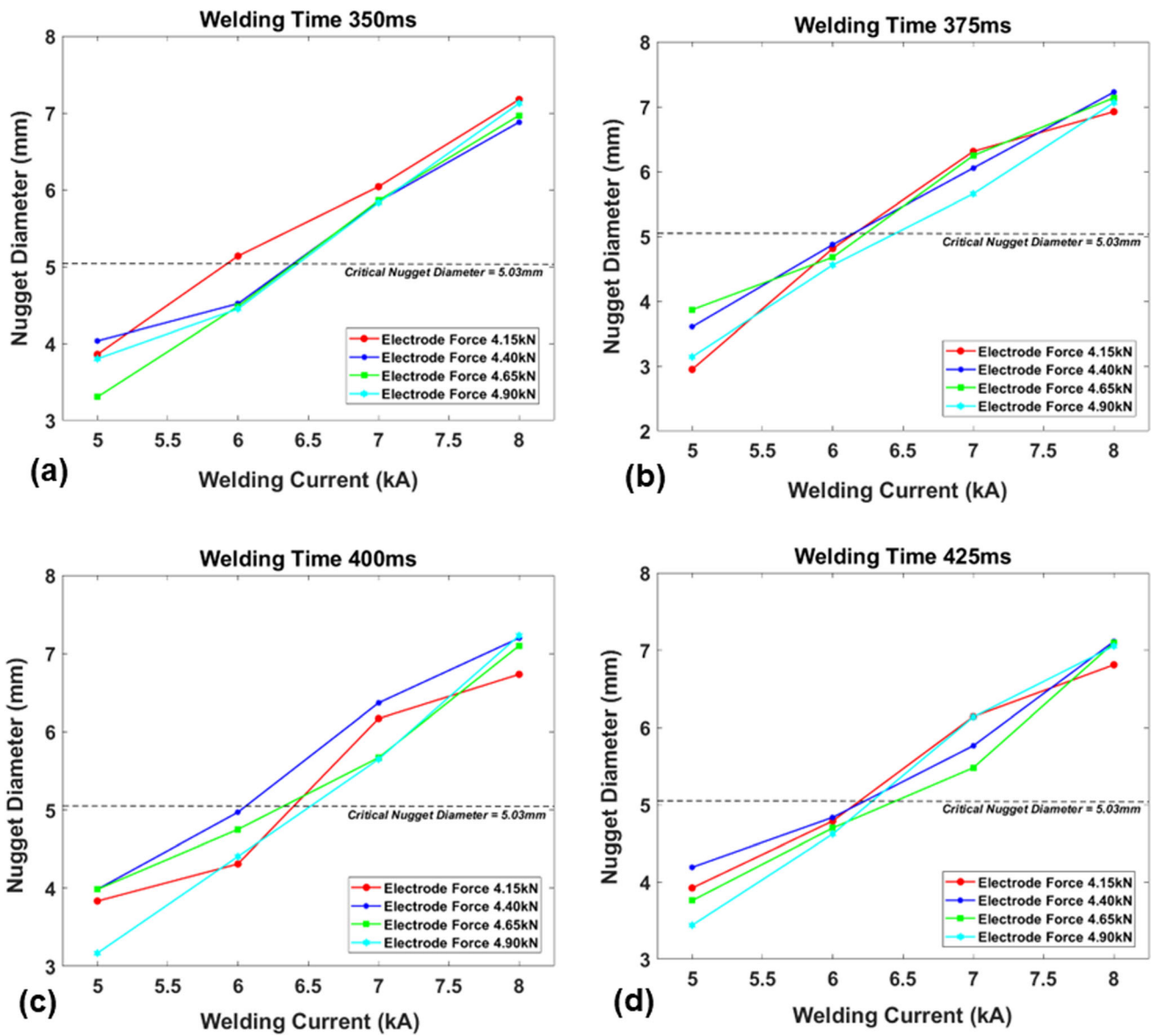
Fig. 6 Relationship between ND and WC

Vernier caliper from the coach peel test samples. The experimental data generated as per the design of experiments are shown in Table A1.

2.3 Prediction Models

The weld quality indicators were predicted using ANN and ANFIS on MATLAB software. The WC, WT, and EF were the input welding parameters considered for the prediction models.

The criteria used to estimate the performance of the ANN and ANFIS models are R-squared (R^2), EP, and mean square error (MSE). It can be noted that the size of the training dataset has a significant impact on the performance of the prediction model. Hence, we have used 54 datasets for training and 10 datasets to validate and test the prediction models.

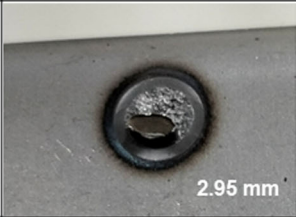For the ANN model, the first layer is the input layer comprised of three input parameters that are connected to two
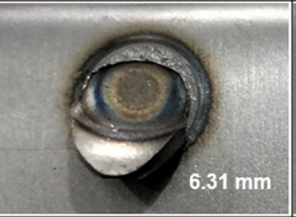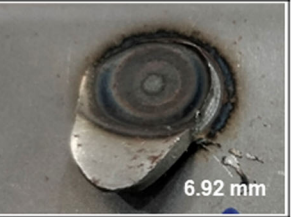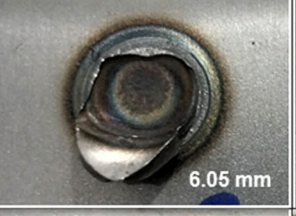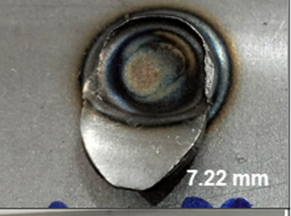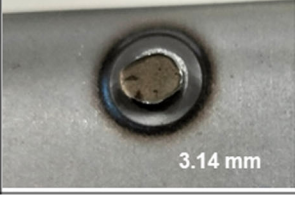
Fig. 7 Effect of WC and EF on the size of the nugget

hidden layers, which consist of six hidden neurons with transfer function hyperbolic tangent sigmoid (tansig) and log-sigmoid (logsig), respectively. The hidden neurons are then connected to the output layer of four neurons with a linear (purelin) transfer function. The gradient descent optimizer was used in the ANN model. The architecture of the ANN model is shown in Fig. 4(a). The back-propagation algorithm used for the training function is the Bayesian regularization algorithm. The output layer consists of the four weld quality indicators. Bayesian regularization was used since it prevents overfitting by incorporating a prior distribution over the model parameters, which encourages the model to have smaller parameter values and thus be less complex. The advantage of Bayesian regularization over other regularization techniques is that it
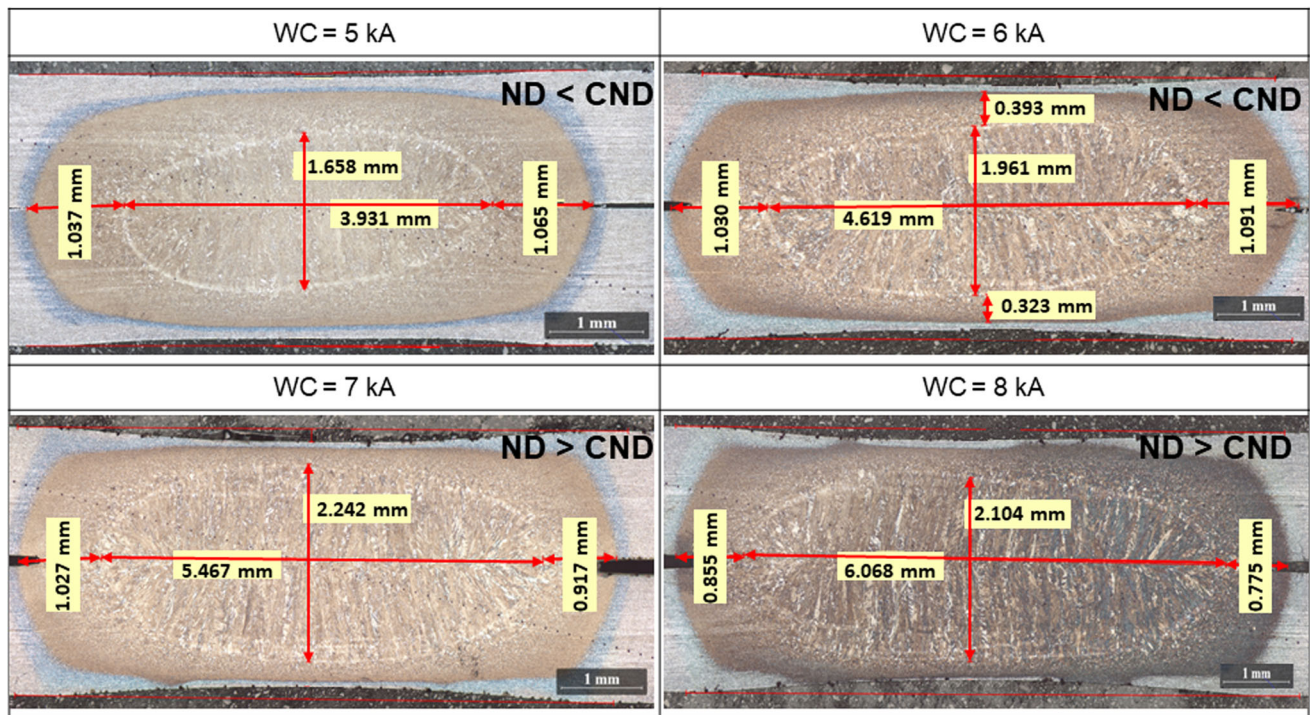
Fig. 8 Macrostructure images illustrating the change in ND with the corresponding increase in WC

allows for the automatic selection of the regularization parameter using Bayesian inference. Hence, there is no need to manually tune the regularization parameter, which can be difficult with small datasets (Ref 36).

Another approach, the ANFIS model, is also used due to its advantages over the ANN model. The ANFIS model integrates the fuzzy inference system with neural networks. Figure 4(b) shows the different layers of the ANFIS algorithm. The ANFIS algorithm uses a set of if–then rules which governs the membership function. The fuzzy inference system is generated using a grid partition. The member function type is the Gaussian membership function (gaussmf) for the input and linear for the output. The number of member functions used for each input is four. The total number of rules used is sixty-four, and the training method used is hybrid. The prediction was made for each weld quality indicator individually.

2.4 Multi-objective Optimization

Most real-world engineering problems consist of several parameters (objectives) that need to be optimized (either maximizing or minimizing) simultaneously, with an equality and inequality constraint attached to each objective (Ref 37,

38). The RSW process parameters, such as WC, WT, and EF, were evaluated and optimized using the multi-objective genetic algorithm (MOGA). The weld quality criteria considered (ND, PS, TSS, and MDCR) have made it feasible to identify the ideal welding settings that produce high-quality welds. The multi-objective optimization was done on MATLAB software. The procedure followed to optimize the welding parameters is shown in Fig. 5. The initial objective equations for the welding parameters were constructed using multivariate regression and are shown in Eq 2-5. The developed models were then tested using analysis of variance (ANOVA) to examine adequacy at 95 percent. The ANOVA for the developed multivariate regression model is shown in Table 5.

$$
\begin{aligned}
ND = {}&-9.5531 + 0.37149(WC) - 0.010251(WT) + 5.5117(EF) + 0.024883(WC)^2 \\
&+ 1.3438 \times 10^{-5}(WT^2) - 0.82312(EF^2) - 0.00091375(WC \times WT) \\
&+ 0.001387(WT \times EF) + 0.17638(EF \times WC)
\end{aligned}
$$

$$(Eq\ 2)$$

$$
\begin{aligned}
PS = {}&9.661 + 3.1638(WC) - 0.16571(WT) + 6.4969(EF) + 0.11728(WC^2) + 0.00032764(WT^2) \\
&- 0.77533(EF^2) - 0.012334(WC \times WT) - 0.00039844(WT \times EF) \\
&+ 0.056607(EF \times WC)
\end{aligned}
$$

$$(Eq\ 3)$$

Welding Current				
5 kA	6 kA	7 kA		8 kA
Interfacial Fracture	Interfacial Fracture	Partial Interfacial Fracture	Interfacial Fracture	Pullout Fracture
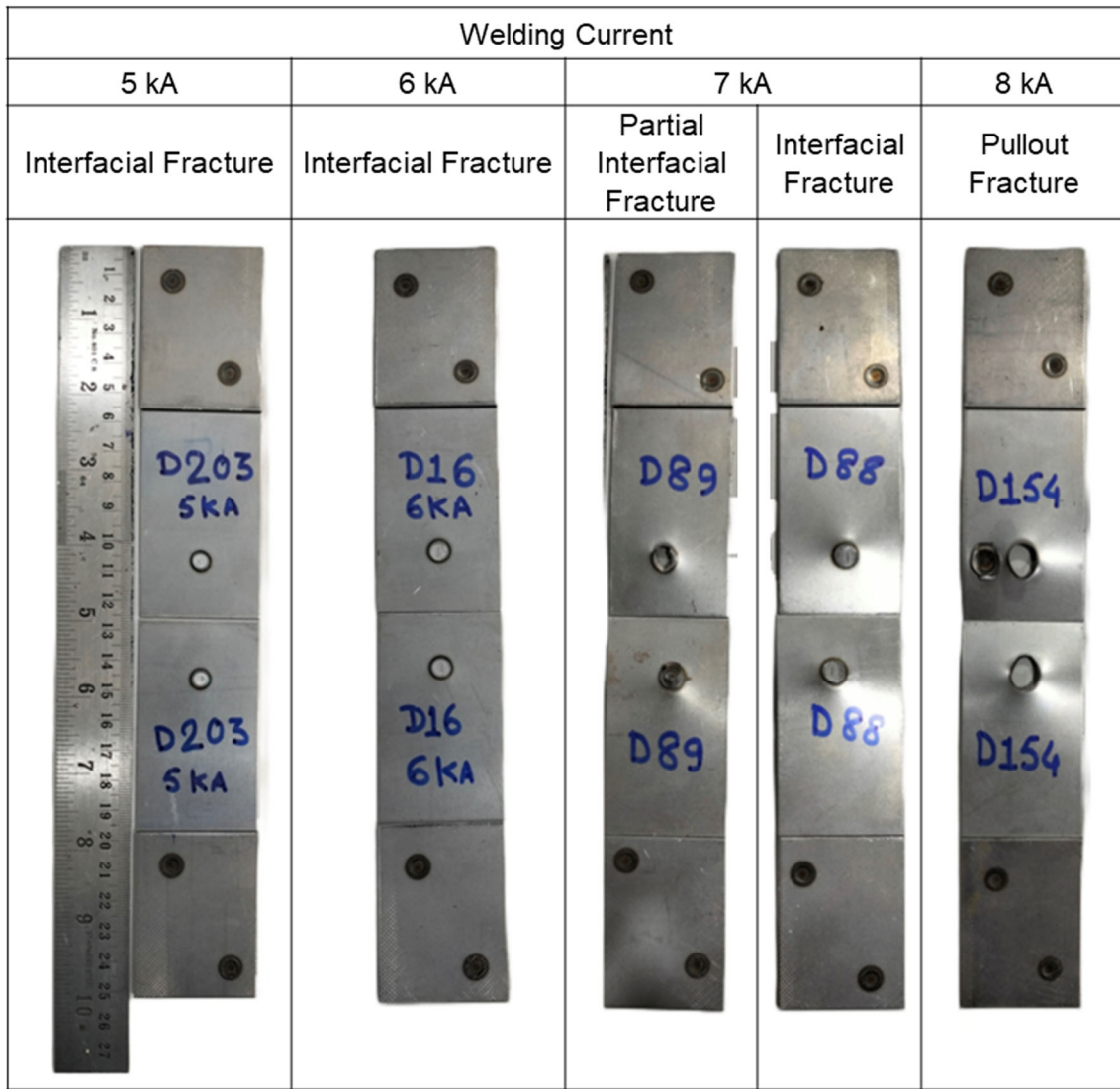
Fig. 9 Failure modes during tensile shear test

$$TSS = -54.93 + 18.165(WC) + 0.094134(WT) - 7.1499(EF)$$
$$- 1.11(WC^2) - 0.00022765(WT^2) \quad - 0.42175(EF^2)$$
$$- 0.0011062(WC \times WT) + 0.021405(WT \times EF)$$
$$+ 0.27481(EF \times WC)$$

$$\text{(Eq 4)}$$

$$MDCR = 821.3 - 45.699(WC) - 1.5945(WT) - 37.511(EF)$$
$$+ 0.44624(WC^2) + 0.001081(WT^2) \quad - 4.8047(EF^2)$$
$$+ 0.010785(WC \times WT) + 0.12199(WT \times EF) + 3.5903(EF \times WC)$$

$$\text{(Eq 5)}$$

The aim and weights assigned for each of the objectives in the multi-objective optimization model are shown in Table 6. The symbol "*" denotes the weight assigned. The higher the number of "*," the more significant the weight assigned to the objective. This approach can be used in the automotive industry to improve weld quality, eliminate defects, and reduce produc-
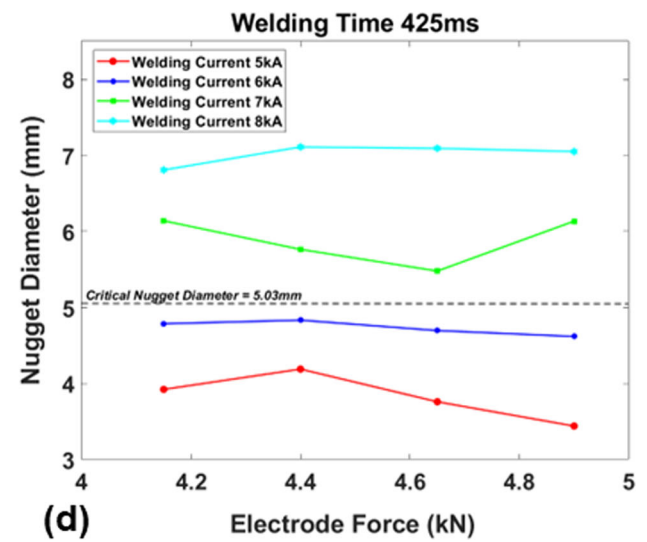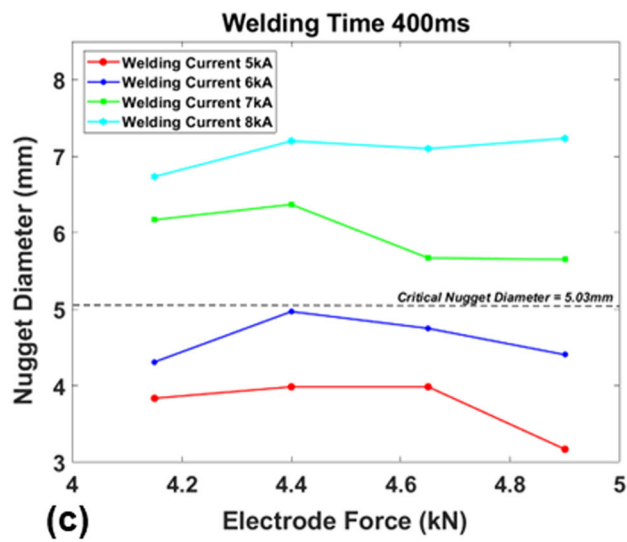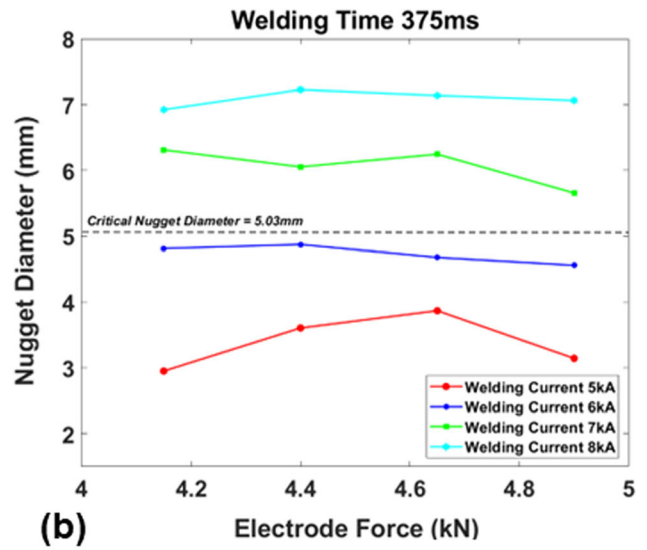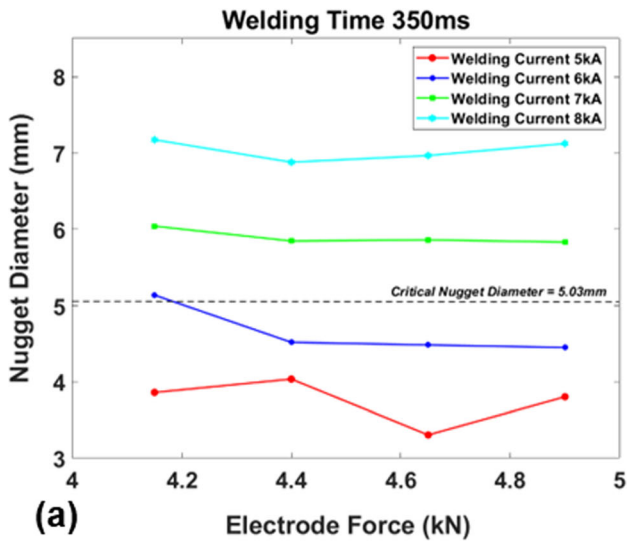
Fig. 10 Relationship between ND and EF

tion time while extending the welding equipment's service life. Then some of the critical GA parameters were selected and set to an appropriate value, as shown in Table 7, to generate the best possible results. The stochastic uniform was used as the selection function mainly because of its ability to maintain diversity within the population. It is also a more efficient selection method than the tournament, roulette wheel, and ranking method since it selects multiple parents at once without any bias applied. The scattered crossover function was used because it allows for the exchange of genetic information across multiple locations in the genome rather than just a single or a few points. This improves the diversity of the offspring and reduces the likelihood of producing infeasible solutions.
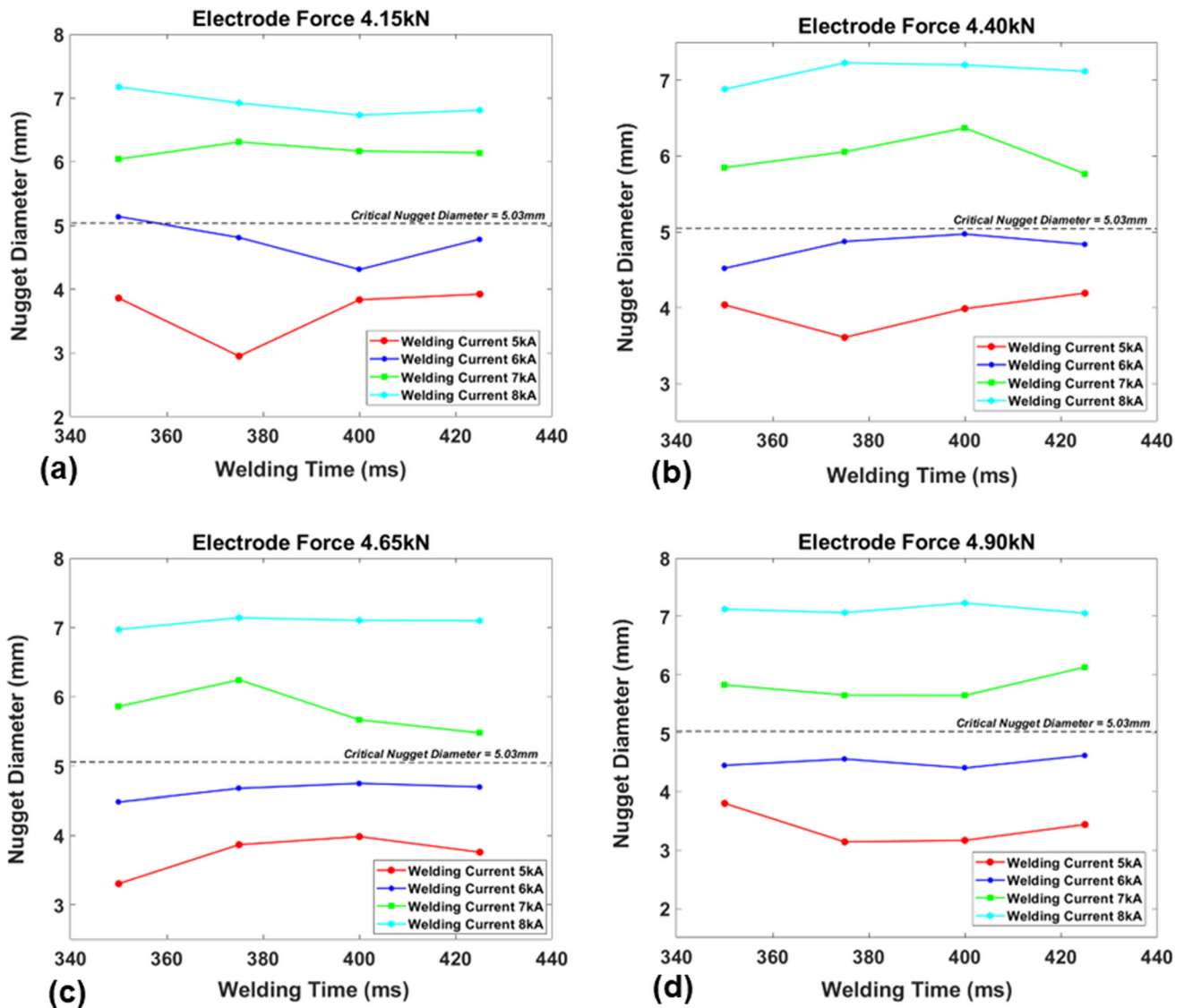
Fig. 11 Relationship between ND and WT

3. Results and Discussion

3.1 Effects of Welding Parameters on Weld Quality

The welding parameters' effect on the weld's quality can be correlated with the weld nugget size since the PS and TSS are directly, and MDCR is inversely proportional to ND. The welding parameters studied here are WC, WT, and EF. The critical nugget diameter (CND) for the RSW of DP780 steel sheets of thickness 1.40 mm is calculated using Eq 6. Here, the CND equals 5.03 mm. When the ND formed is less than the CND, an interfacial failure is dominant when loads are applied, whereas when the ND is greater than the CND, the dominant failure mode is a button failure or a pullout failure (Ref 39). The pullout failure is the preferred failure mode for spot welds because the energy dissipated by the non-straight path of crack propagation is higher than the energy dissipated during interfacial failure (Ref 40).

$$CND = 4.25 \times \sqrt{th} \tag{Eq 6}$$

where th = thickness of the sheet (mm).

The effect of the variation in WC on the ND, as shown in Fig. 6, indicates that the ND is directly proportional to the WC.
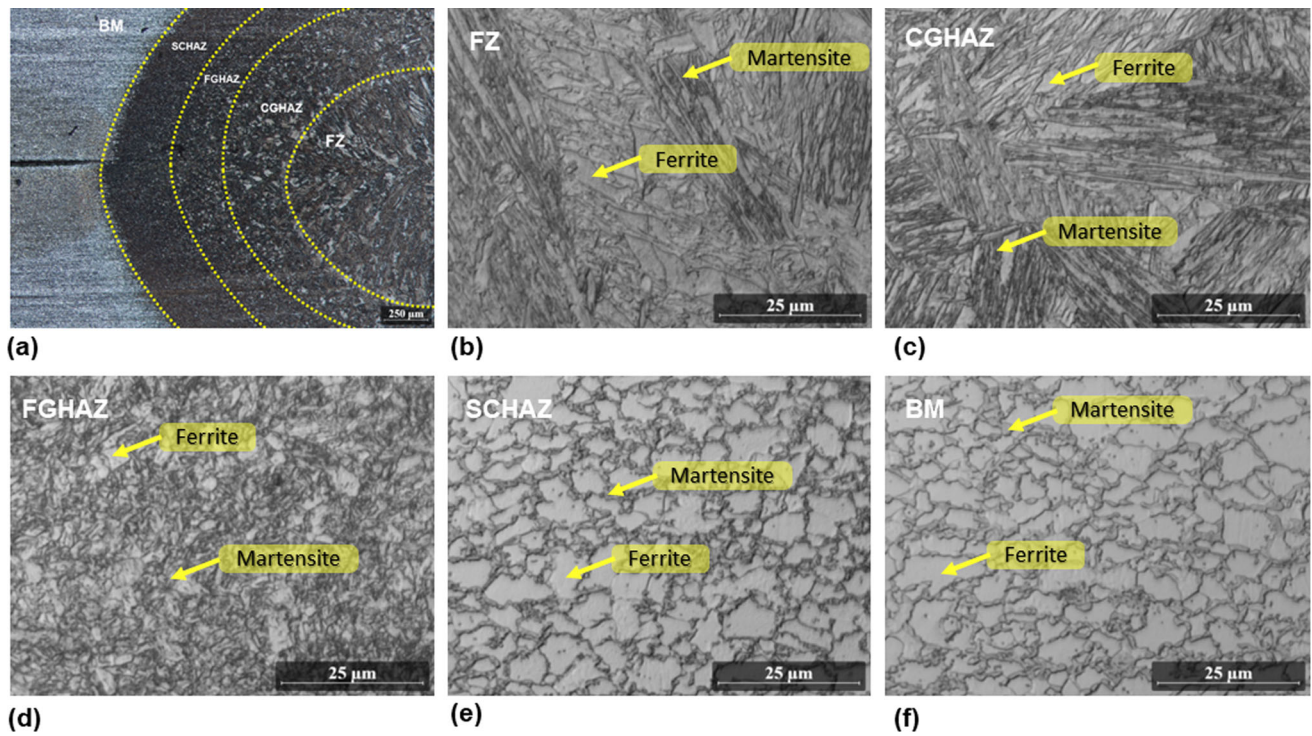
Fig. 12 (a) Macrostructure of the weld nugget cross section, (b) FZ, (c) CGHAZ, (d) FGHAZ, (e) SCHAZ, (f) BM

The ND continuously increases with the corresponding increase in the WC up to the maximum intensity tested (8.0 kA). This phenomenon occurs because the ND mainly depends on the amount of heat generated. From Eq 1 (Joule's law), it is evident that the heat produced is directly correlated with the square of the WC passing through the electrode. The trend of ND increasing with an increase in WC is also visible in Fig. 7, which illustrates the effects of WC and EF on the size of the nugget.

Figure 6 shows that when the WC is lesser than 6.5 kA, the ND obtained is below the CND. Hence, the critical WC for DP780 steel sheets of 1.40 mm thickness is 6.5 kA. This trend is also visible in Fig. 8 and is in line with the results obtained by other researchers (Ref 33, 39, 41). Figure 9 shows the failure modes of the welded samples during the tensile shear test. When 8 kA WC is used, the failure mode is always pullout fracture which is much more desirable than interfacial fracture, which is observed at lower WC.

Most researchers studying the RSW of steels report that there is a WC threshold above which the ND decreases due to expulsion (Ref 42). The findings indicate that the WC threshold for the applied EF of 4.15 kN was achieved because slight expulsion was observed at a WC of 8.0 kA. There was a slight reduction in the ND, as shown in Fig. 6 and 7. Several

researchers claim that increasing the EF can also increase the WC without expulsing material (Ref 43, 44). A similar trend was noticed in this study. Minor expulsions were observed when WC of 8 kA and EF of 4.15 kN were used, but expulsion was eliminated as the EF was increased to 4.40 kN. When a low EF of 4.15 kN was applied, and a WC of 5 kA to 7 kA was used, a partial interfacial failure of the nugget was observed during the coach peel test. When a WC of 8 kA is used, a pullout failure is constantly observed, and the sheet metal surrounding the nugget fails. WC greater than 7 kA produces a nugget with an ND greater than the CND of 5.03 mm. When the ND exceeds the CND, the dominant failure mode observed is a pullout failure.

Figure 10 depicts the relationship between the ND and the EF. The increase in EF leads to an increase in the ND till a critical EF of 4.40 kN. The ND gradually decreases when the EF increases to a value greater than 4.40 kN. The explanation for this phenomenon would be that due to an increase in the EF above a critical value (in this case, 4.40 kN), the minute gaps between the two steel sheets will be reduced, significantly improving the contact patch between the two faying surfaces. This, in turn, drastically reduces the electrical resistance and the heat generated (Ref 39, 42). However, when the EF is greater than 4.40 kN, the electrode indentation increases, further
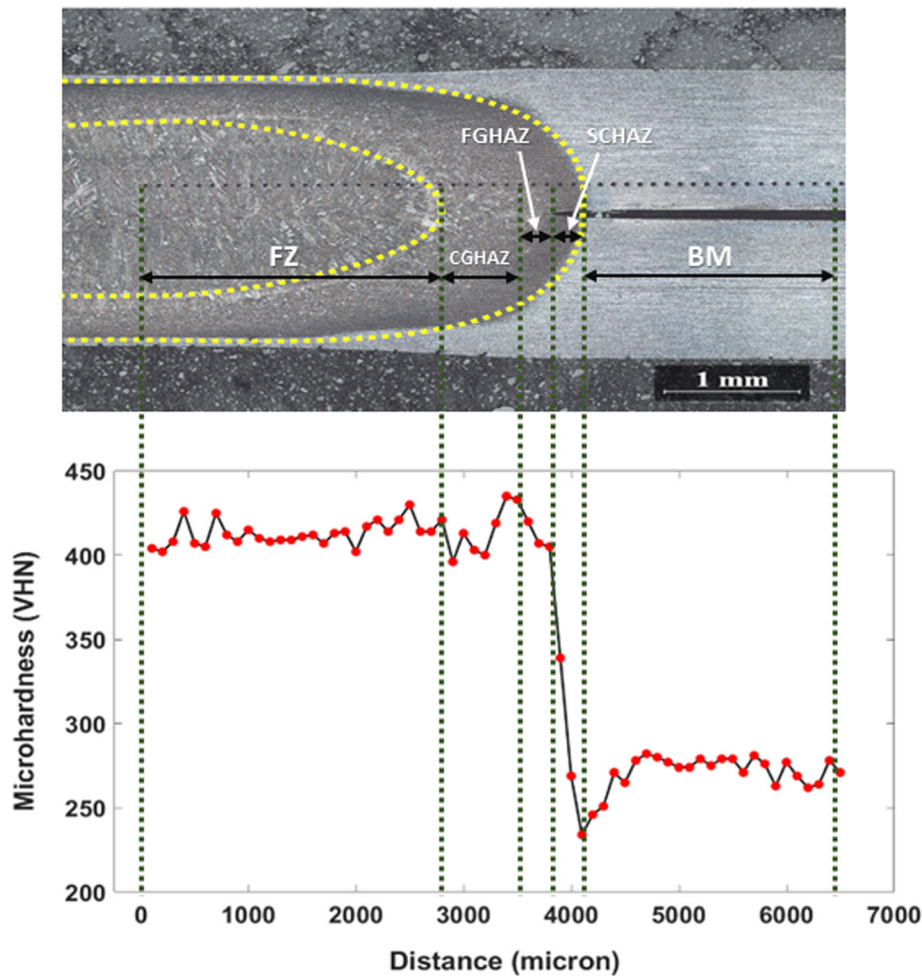
Fig. 13 Vickers microhardness profile across one-half of the weld region

reducing the electrical resistance and decreasing the ND (Ref 45-47). This decrease in the electrical resistance, which leads to lower heat generation, can be counteracted by adjusting the other welding parameters. Either the WC or the WT or both the WC and WT should be increased to compensate for the heat lost when a high EF is used.

As the WT is increased, there is only a slight increase in the overall ND, as shown in Fig. 11. The WT has a negligible effect on the ND (Ref 47, 48). Figure 11 shows that there is only a marginal increase in ND as the WT increases but a drastic increase in ND as the WC increases. However, it can be noted that the excess heat generated due to the longer WT results in a higher weld indentation which explains the lack of significant increase in the ND (Ref 42, 49). The increase in WT can drastically increase the contact surface temperature, increasing

melting in the contact zone without any melt spatter. Increasing the WT brings the weld pool to a state of equilibrium which restricts the growth in the nugget (Ref 50).

3.2 Microstructure and Microhardness

The microstructure of the RSW DP780 steel weld specimens is shown in Fig. 12. The welded region is analyzed, and the distinct zones formed due to the different local peak temperatures and cooling rates are studied. Figure 12(b) shows the fusion zone (FZ) microstructure. In the FZ, the base material (BM) melts as the heat generated between the two faying surfaces of the sheets is much higher than the melting point of the steel. In contrast to the BM microstructure, the FZ had higher martensite content due to the higher local peak
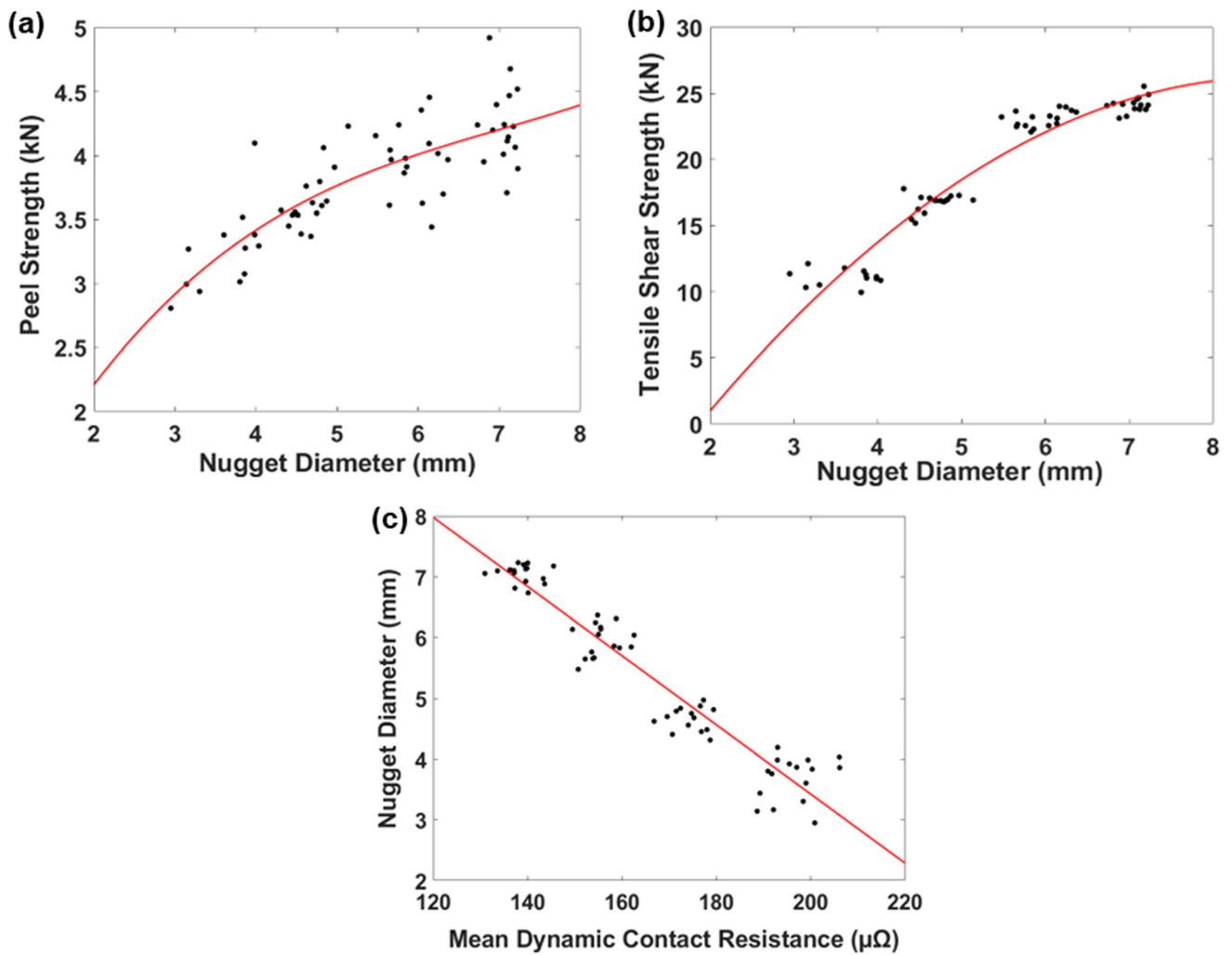
Fig. 14 (a) PS as a function of ND; (b) TSS as a function of ND; (c) ND as a function of MDCR

Table 8 Comparison between the actual and predicted values of ND

Sl. no.	Process parameters			Actual	ANN prediction			ANFIS prediction		
	WC, kA	WT, ms	EF, kN	ND, mm	ND, mm	EP, %	Error^2	ND, mm	EP, %	Error^2
1	5	375	4.15	2.950	2.972	0.736	0.0005	2.950	0.0000	0.00E+00
2	5	400	4.40	3.985	3.988	0.078	0.0000	3.985	0.0025	1.00E−08
3	6	350	4.40	4.518	4.498	0.427	0.0004	4.518	0.0132	3.60E−07
4	6	375	4.90	4.558	4.504	1.167	0.0028	4.558	0.0087	1.60E−07
5	7	350	4.40	5.845	5.876	0.530	0.0010	5.845	0.0000	0.00E+00
6	7	425	4.15	6.140	6.210	1.145	0.0049	6.140	1.4E−14	7.89E−31
7	8	350	4.65	6.968	6.877	1.298	0.0082	6.968	0.0086	3.60E−07
8	8	425	4.40	7.113	7.007	1.485	0.0112	7.113	0.0084	3.60E−07
9	6	425	4.90	4.620	4.641	0.461	0.0005	4.620	0.0021	1.00E−08
10	6	350	4.15	5.138	5.173	0.699	0.0013	5.138	0.0116	3.60E−07
					Mean	0.8025	0.0031		0.0055	1.62E−07

Table 9 Comparison between the actual and predicted values of PS

Sl. No.	Process parameters			Actual	ANN prediction			ANFIS prediction		
	WC, kA	WT, ms	EF, kN	PS, kN	PS, kN	EP, %	Error^2	PS, kN	EP, %	Error^2
1	5	375	4.15	2.806	2.874	2.409	0.0046	2.806	0.000	0.00E+00
2	5	400	4.40	3.381	3.386	0.145	0.0000	3.381	1.31E−14	1.97E−31
3	6	350	4.40	3.534	3.521	0.359	0.0002	3.534	0.000	0.00E+00
4	6	375	4.90	3.387	3.400	0.375	0.0002	3.387	0.000	0.00E+00
5	7	350	4.40	3.978	4.018	1.028	0.0017	3.978	0.015	3.60E−07
6	7	425	4.15	4.456	4.440	0.364	0.0003	4.456	1.99E−14	7.89E−31
7	8	350	4.65	4.399	4.365	0.768	0.0011	4.399	0.000	0.00E+00
8	8	425	4.40	4.145	4.202	1.375	0.0033	4.145	0.014	3.60E−07
9	6	425	4.90	3.760	3.694	1.763	0.0044	3.760	0.003	1.00E−08
10	6	350	4.15	4.230	4.217	0.298	0.0002	4.230	2.09E−14	7.89E−31
					Mean	0.8885	0.0016		0.0032	7.30E−08

Table 10 Comparison between the actual and predicted values of TSS

Sl. No.	Process parameters			Actual	ANN prediction			ANFIS Prediction		
	WC, kA	WT, ms	EF, kN	TSS, kN	TSS, kN	EP, %	Error^2	TSS, kN	EP, %	Error^2
1	5	375	4.15	11.355	11.360	0.044	0.000	11.355	0.000	0.00E+00
2	5	400	4.40	11.118	11.112	0.052	0.000	11.118	0.005	2.50E−07
3	6	350	4.40	17.112	17.083	0.167	0.001	17.112	0.002	1.60E−07
4	6	375	4.90	15.932	15.975	0.272	0.002	15.932	0.001	1.00E−08
5	7	350	4.40	23.225	23.186	0.165	0.001	23.225	0.002	1.60E−07
6	7	425	4.15	23.119	23.055	0.276	0.004	23.118	0.000	1.00E−08
7	8	350	4.65	23.256	23.306	0.218	0.003	23.256	0.002	1.60E−07
8	8	425	4.40	24.666	24.800	0.546	0.018	24.666	0.004	8.10E−07
9	6	425	4.90	17.059	17.102	0.252	0.002	17.059	0.000	1.26E−29
10	6	350	4.15	16.914	16.957	0.254	0.002	16.914	0.001	4.00E−08
					Mean	0.225	0.0033		0.0016	1.60E−07

temperature and much faster cooling rates. The FZ is cooled rapidly using the water-cooled copper alloy electrodes, quickly dissipating heat.

The following distinct zone present is the heat-affected zone (HAZ). The HAZ is an intermediate zone between the FZ and BM where the heat produced is not high enough to melt the material but just enough to alter its microstructure. Due to the directional solidification phenomenon in metals, the grains of the HAZ grow from the FZ toward the BM. Due to this phenomenon, different grain sizes are observed at different parts of the HAZ. Based on the difference in grain size, the HAZ can be further divided into three distinct zones that are coarse-grained heat-affected zone (CGHAZ), fine-grained heat-affected zone (FGHAZ), and subcritical heat-affected zone (SCHAZ), which are shown in Fig. 12(c), (d), and (e) respectively. The CGHAZ is the closest to the FZ and has a higher martensitic content than FGHAZ and SCHAZ. The SCHAZ is furthest away from the FZ and has the lowest martensite content compared to the CGHAZ and FGHAZ. The heat the resistance produces does not affect the BM due to its distance from the FZ. The microstructure of the BM shows the typical DP780 microstructure where the martensite is dispersed in a ferritic matrix at the grain boundaries, as shown in Fig. 12(f).

The microhardness of the DP780 welded specimen was studied, as shown in Fig. 13. The presence of martensite content increases the hardness of the material. The maximum hardness of 435 VHN is found at the CGHAZ and the FGHAZ
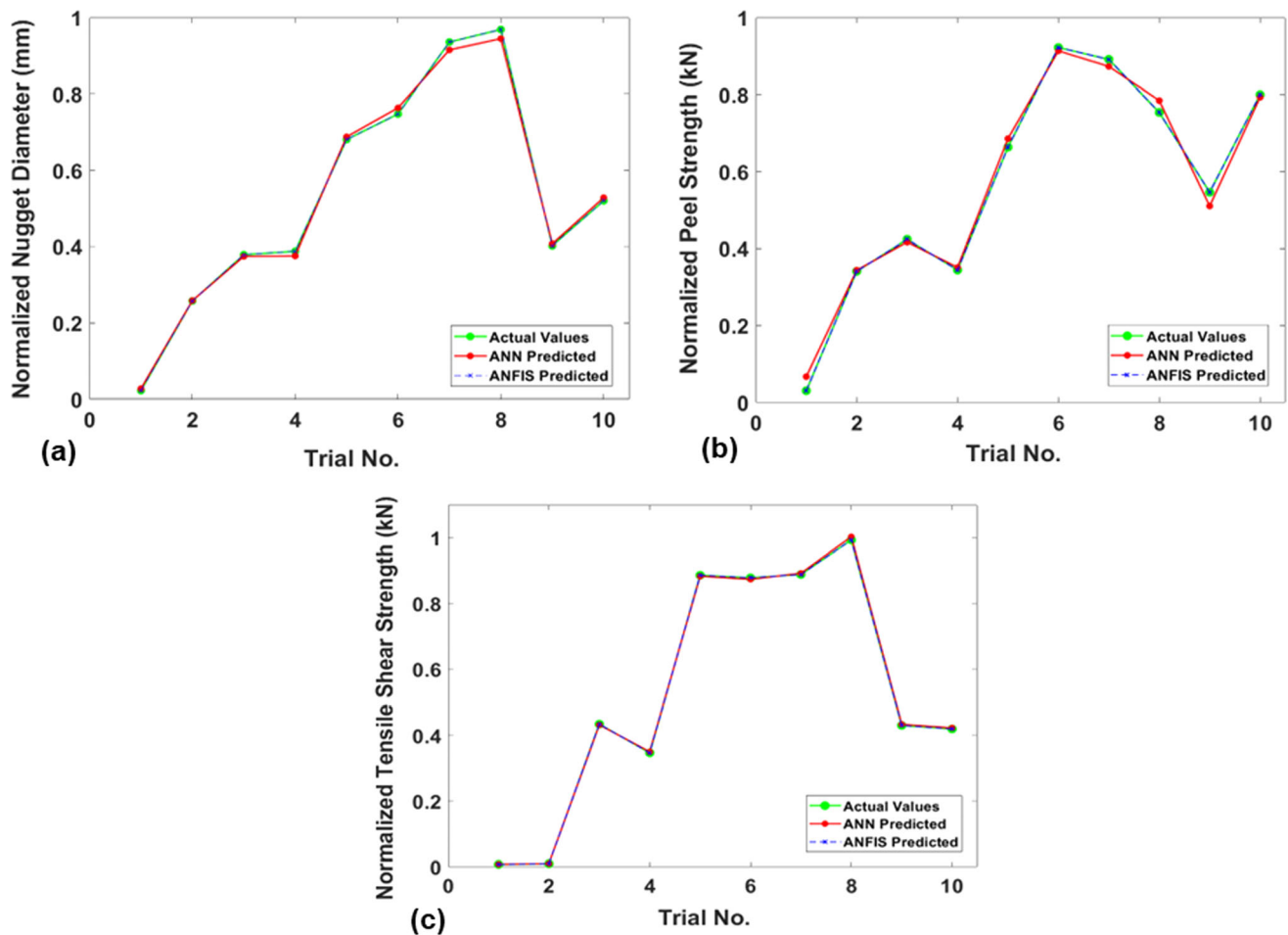
Fig. 15 Comparison between the actual and predicted responses from ANN and ANFIS (a) ND (b) PS (c) TSS

interface. This is due to smaller and finer martensite grains compared to the FZ. The SCHAZ is subjected to high temperatures during welding but does not experience the full melting. The prolonged exposure to elevated temperatures causes the microstructure in the SCHAZ to undergo thermal cycles and experience grain growth, which leads to a less ordered coarse microstructure and tempering of martensite in this region. This results in a steep drop in the microhardness at the SCHAZ. The BM has the lowest microhardness value of 234 VHN because it contains the least amount of martensite.

3.3 Relationship Between the Weld Quality Indicators

For welding process optimization, a polynomial regression analysis was performed to study the relationships between the chosen weld quality parameters (ND, PS, TSS, and MDCR). Figure 14(a) and (b) shows the variation in the PS and TSS with the corresponding change in ND and follow a second-order polynomial fit with an R^2 value of 0.6599 and 0.9214, respectively. It is evident that the PS and TSS increase with an enhancement in the ND, but the rate of increase flatlines beyond a specific value of ND. The results agree with Pouranvari et al., who observed a similar increase in PS and TSS with the corresponding increment in the ND for DP600 RSW joints (Ref 51). Since tensile shear tests offer better data

Table 11 Optimized solutions for ND, PS, TSS, and MDCR

| Sl. no.	Welding process parameters				Weld quality indicators		
	WC, kA	WT, ms	EF, kN	ND, mm	PS, kN	TSS, kN	MDCR, $\mu\Omega$
1	6.24	369.36	4.89	5.56	3.47	20.96	160.01
2	6.30	374.17	4.90	5.71	3.58	21.20	156.58
3	8.00	396.88	4.90	7.01	4.55	24.28	135.77
4	7.40	352.22	4.81	6.32	4.08	22.82	148.08
5	6.15	381.24	4.89	5.07	3.27	19.12	166.80
6	7.39	354.38	4.83	6.31	3.90	22.84	148.44
7	7.25	351.23	4.87	6.09	3.84	22.06	150.07
8	6.43	360.74	4.90	5.05	3.20	19.09	165.95
9	7.29	391.12	4.90	6.12	3.78	22.63	149.20
10	6.62	385.94	4.90	5.29	3.38	20.49	161.60
11	8.00	350.62	4.90	7.05	4.75	24.55	136.51
12	6.81	384.52	4.89	5.54	3.44	21.03	156.33
13	7.07	361.49	4.90	5.84	3.76	21.74	154.26
14	6.40	373.58	4.89	5.03	3.32	19.28	164.92
15	7.18	358.83	4.89	6.00	3.90	22.07	152.76
16	6.58	367.27	4.90	5.24	3.41	19.96	162.28
17	6.87	388.25	4.89	5.61	3.46	21.18	155.00
18	7.08	362.00	4.90	5.86	3.76	21.80	153.98
19	6.32	360.25	4.89	5.35	3.36	20.29	162.26
20	7.38	387.52	4.88	6.25	3.94	22.74	147.16
21	6.63	372.69	4.89	5.31	3.41	20.33	160.79
22	6.69	381.08	4.89	5.38	3.40	20.72	158.90
23	6.20	360.49	4.85	5.51	3.52	20.59	160.16
24	8.00	358.78	4.88	7.05	4.81	23.82	136.64
25	7.69	368.36	4.90	6.63	4.39	23.60	142.52
26	7.97	365.25	4.87	7.01	4.44	24.04	138.37
27	6.85	372.75	4.89	5.57	3.50	21.02	156.94
28	7.96	388.20	4.87	6.98	4.50	24.24	136.31
29	7.93	355.99	4.87	6.96	4.58	23.75	138.39
30	6.22	382.70	4.87	5.64	3.31	18.56	158.57

repeatability and reliability than coach peel tests, less scatter is shown in Fig. 14(b) than in Fig. 14(a); this is because the peak load in the coach peel test is less sensitive to the size of the fusion zone than in tensile shear tests (Ref 52, 53).

Figure 14(c) shows the relationship between ND and MDCR. As the MDCR rises, the corresponding ND decreases linearly, and this interaction can be quantified using a linear fit with an R^2 value of 0.9128. Hence, a clear conclusion can be drawn that the ND is inversely proportional to the MDCR (Ref 54). Therefore, ND should be maximized, and MDCR should be minimized to maximize the weld strength.

3.4 Prediction of Weld Quality Indicators

The prediction of the weld quality was made using ANN and ANFIS. In both methods, experimental data (54 datasets) was used as training data to train the neural network, and another set of experimental data (10 datasets) was used to test and validate the predictions made by the algorithm. The validation metrics used were the EP and mean square error (MSE) in the predictions made by the algorithm. The prediction was made for each output weld quality indicator separately with
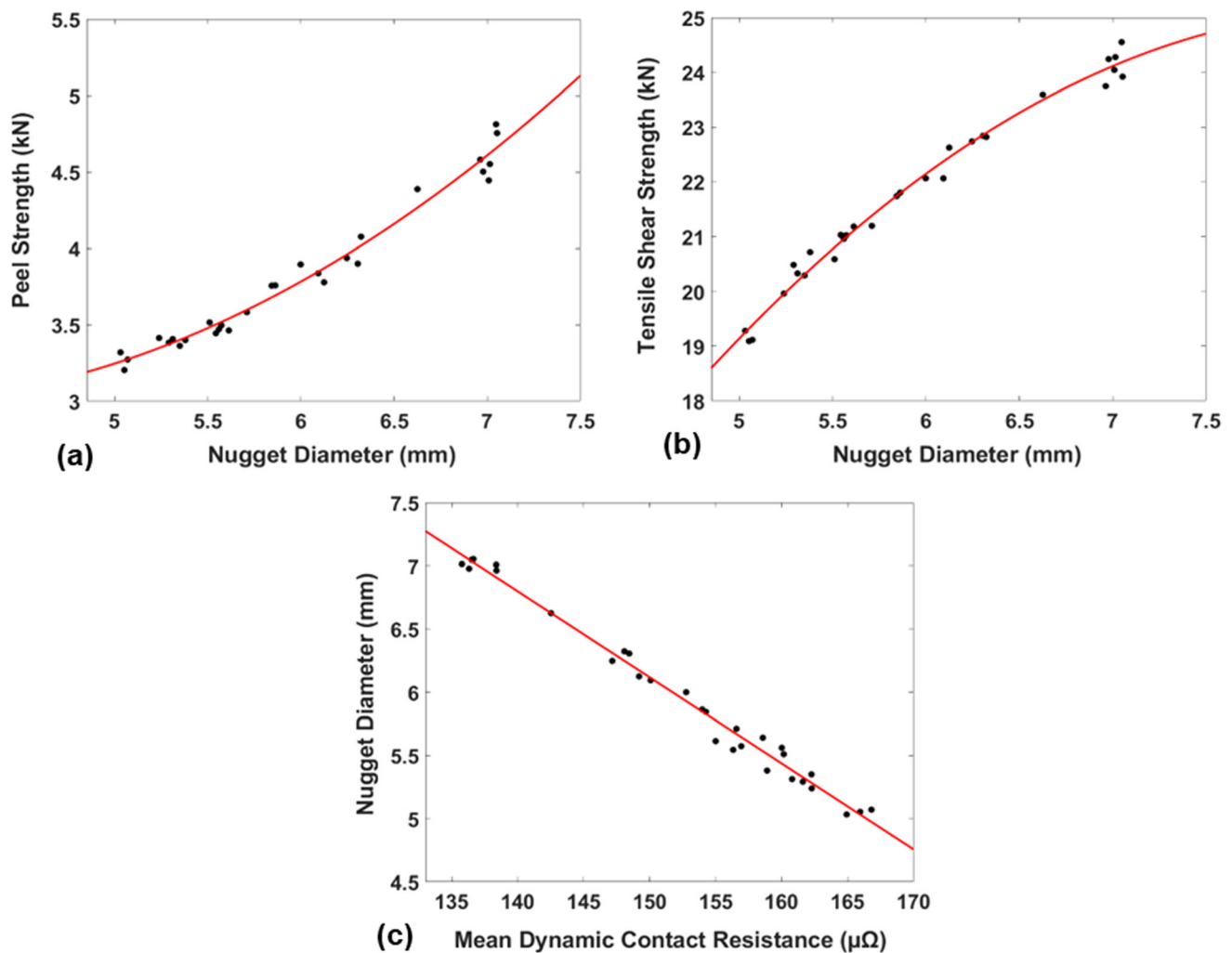
Fig. 16 Relationship between the Pareto optimal set of weld quality indicators (a) PS, (b) TSS as a function of ND, (c) ND as a function of MDCR

the set of input welding parameters to improve the efficiency and reduce the algorithm's complexity.

Tables 8, 9, and 10 show the EP and the MSE for the predictions made using ANN and ANFIS models for ND, PS, and TSS, respectively, as these are the main outputs monitored by the automotive companies. The EP ranges for ND were recorded as 0.0778 to 1.4847 with ANN and 0 to 0.0132 with ANFIS. Therefore, ANFIS is found to be precisely predicting the ND. Similarly, the EP range for PS and TSS with ANN was 0.1449 to 2.4091 and 0.0440 to 0.5461, respectively. The ANN algorithm could predict the TSS output with very high accuracy; this can be attributed to the lesser deviations observed in the experimental data. Due to a noticeable scatter in the experimental data for PS and ND, the prediction output has a higher EP.

Similarly, the EP range of the prediction of PS and TSS with ANFIS is 0 to 0.015 and 0 to 0.0045, respectively. Therefore, ANFIS exhibits higher accuracy as compared to ANN. This can be attributed to ANFIS being a comparatively more advanced algorithm as it uses both ANN and fuzzy inference systems to make predictions (Ref 41, 54).

In the ANN model, the algorithm learns the relationship between the input and output (Ref 55). Unlike the ANN algorithm, where the process is done in hidden layers, in the ANFIS model, the process occurs in the mode of if–then statements, where the fuzzy inference algorithm connects the

Table 12 Comparison between the initial and optimized welds

Sl. No.	Input responses		Initial level	24th Pareto solution (Highest PS)				11th Pareto solution (Highest TSS)			
				Optimized level			Gain, %	Optimized level			Gain, %
1.	WC	(kA)	7	8			...	8			...
2.	WT	(ms)	425	358.78			15.58	350.62			17.50
3.	EF	(kN)	4.65	4.88			...	4.90			...
	Output responses			Predicted	Actual		Gain, %	Predicted	Actual		Gain, %
1.	ND	(mm)	5.48	7.05	7.08		28.64	7.05	7.12		28.64
2.	PS	(kN)	4.15	4.81	4.79		15.90	4.75	4.67		14.46
3.	TSS	(kN)	20.21	23.82	23.84		17.86	24.55	23.80		21.47
4.	MDCR	(μΩ)	150.70	136.64	137.23		...	136.51	139.56		...

inputs to the desired output. This method increases the ease of understanding and making changes to the algorithm. Figure 15 shows the normalized values of the actual and predicted output responses from the ANN and ANFIS models. Therefore, it is evident that ANFIS is better for predicting output than ANN (Ref 41, 54, 56).

Furthermore, it can be summarized that the ANFIS was more accurate than the ANN for predicting weld quality indicators. The accuracy of ANFIS (99.98%) is superior to ANN (99.36%) during the prediction of all the output responses. This can be attributed to the architecture of the ANFIS model. ANFIS is a hybrid model which combines neural networks with a fuzzy interference system. This improves the model's speed, efficiency, fault tolerance, and adaptiveness. This makes ANFIS models more interpretable and transparent than ANN models, as the fuzzy rules can be understood and analyzed by experts in the field. This is especially valuable in RSW, where expert knowledge can provide insights into the complex relationships between the input welding parameters and the weld quality indicators. The hybrid structure of ANFIS allows for both numerical learning (through neural network weights adjustment) and rule-based learning (through fuzzy rule tuning). This can be advantageous in capturing complex nonlinear relationships and optimizing the model's performance. ANFIS models can also handle uncertainty and errors in the training datasets through fuzzy logic. The fuzzy inference system within ANFIS allows for the representation and reasoning of incomplete or uncertain information, providing a more robust framework for modeling and prediction when faced with data imperfections.

3.5 Multi-objective Optimization of the Welding Parameters

The multi-objective optimization was performed on MA-TLAB software using the GA. The optimization goal is to either maximize or minimize the welding process parameters. ND, PS, and TSS were classified as "Higher the better," and MDCR was classified as "Lower the better." Another constraint added to the algorithm was that the optimal Pareto solutions for ND should have a minimum critical ND of 5.03 mm. After several generations, the GA operations no longer significantly influence the improvement of the solutions generated. In this case, it happened in the 149th generation. The outcomes from this generation are regarded as the optimized Pareto set of solutions. The complexity of the goal functions, the size of the population, the constraints applied, and the likelihoods of mutation and crossover all affect the number of generations produced. After optimization, a Pareto optimal set of solutions are generated, and the ideal welding parameters are summarized as shown in Table 11. The best solution among the generated Pareto optimal set of solutions must be determined per the manufacturer's needs.

Figure 16 illustrates the relationship between the optimized set of weld quality indicators. It can be observed that initially, in Fig. 14, the points were relatively more spread out as compared to the points in Fig. 16. This shows that the GA has successfully optimized the welding process parameters to ensure the outputs are more predictable and has generated the optimal set of solutions to achieve better weld strength.

Out of the Pareto set of optimal solutions in Table 11, the best solution to achieve a high PS and TSS is the 24th and the 11th Pareto solution, respectively. Table 12 shows the comparison between the optimal weld quality parameters and the initial

Table 13 Initial and optimal process parameters to achieve minimum TSS of 11.056 kN

Sl. no.	Welding process parameters	Unit	Initial process parameters	Optimized process parameters
1.	WC	kA	6	6.22
2.	WT	ms	425	382.70
3.	EF	kN	4.65	4.87

level of the weld quality parameters and the comparison between the predicted and actual output responses for ND, PS, and TSS. The initial level here is the welding parameters generally used by manufacturers for the RSW of 1.40 mm DP780 steel sheets. From Table 12, it is visible that there is a significant increase in the ND, which results in increased PS and TSS of the weld joints. The gains observed in PS and TSS are comparable to the results of other researchers (Ref 47, 57). The error in the output responses' predicted and experimentally obtained values are within a tolerable limit of less than 1%. This is in line with the findings of other researchers using the GA (Ref 38, 58-60).

Based on the multi-objective optimization results, validation trails were also performed with some of the optimized welding process parameters from the Pareto set of solutions. The CND for 1.4-mm-thick DP780 steel sheets, as per JIS Z3140:2017 standard, is 5.03 mm. The minimum TSS to be achieved and set for the experimental validation was 11.056 kN. The 30th Pareto solution from Table 11 is used. The comparison between the optimal and the experimental welding process parameters is shown in Table 13. Furthermore, from Tables 12 and 13, it is concluded that the welding cycle time of the RSW process has also been considerably reduced by using the optimized welding parameters. This will be crucial for manufacturing companies to improve the productivity and efficiency of the production process.

4. Conclusion

The current study aimed to develop and implement ANN and ANFIS models to predict RSW quality indicators (ND, PS, and TSS) for DP780-DP780 steel sheets of 1.40 mm thickness. The data required to train the ML models were generated using a four-level full factorial design of the experiment. Furthermore, multivariate regression analysis coupled with the GA was used to optimize and generate a set of optimum welding process parameters. The findings of the current study are as follows:

1. The nugget diameter (ND) is directly proportional to the welding current when all the other welding process parameters are kept constant. In contrast, the welding time and electrode force are directly proportional to the nugget diameter till a specific point before the trend is reversed.
2. The mean dynamic contact resistance (MDCR) is inverse to the nugget diameter.

3. The ANN and ANFIS models are reliable and accurate for predicting weld quality. However, the ANFIS model predictions were slightly more accurate than the ANN model. The prediction accuracy of the ANFIS model was higher than 99.98% for all the outputs compared to the ANN model (99.36 %).
4. Multivariate regression analysis confirms that the welding current's impact on the weld quality is the most significant. The undersized nugget formation is observed for 5 kA and 6 kA welding currents. However, for all the cases, 7 and 8 kA welding currents resulted in increased nugget diameter ($>$ critical ND of 5.03 mm).
5. To achieve high weld strength and low cycle time, the optimal set of welding process parameters chosen from the optimal solutions generated using the genetic algorithm (GA) is 8 kA welding current, 350.53 ms of welding time, and 4.89 kN electrode force which produces a weld with a nugget diameter of 7.06 mm, peel strength (PS) of 4.83 kN and tensile shear strength (TSS) of 23.67 kN.

Data Availability

The experimental data generated and analyzed in the current work are available with the authors.

Conflict of interest

The authors declare no conflict of interest.

Appendix

See Table 14.

Table 14 Experimental data generated based on the design of experiments.

Sl. No.	Welding parameters			Output parameters			
	WC, kA	WT, ms	EF. kN	ND, mm	PS, kN	TSS, kN	MDCR, $\mu\Omega$
1	5	350	4.15	3.86	3.07	11.27	206.13
2	5	350	4.40	4.04	3.29	10.85	206.06
3	5	350	4.65	3.31	2.94	10.50	198.40
4	5	350	4.90	3.80	3.01	9.94	190.92
5	5	375	4.15	2.95	2.81	11.36	200.84
6	5	375	4.40	3.61	3.38	11.78	198.99
7	5	375	4.65	3.87	3.28	11.02	197.02
8	5	375	4.90	3.14	2.99	10.31	188.64
9	5	400	4.15	3.84	3.52	11.56	200.30
10	5	400	4.40	3.99	3.38	11.12	199.42
11	5	400	4.65	3.99	4.10	10.98	192.93
12	5	400	4.90	3.17	3.27	12.12	192.10
13	5	425	4.15	3.92	5.94	11.55	195.47
14	5	425	4.40	4.19	6.01	11.75	192.97
15	5	425	4.65	3.76	5.28	11.41	191.76
16	5	425	4.90	3.44	4.90	10.84	189.23
17	6	350	4.15	5.14	4.23	16.91	201.40
18	6	350	4.40	4.52	3.53	17.11	200.46
19	6	350	4.65	4.48	3.56	16.22	177.99
20	6	350	4.90	4.45	3.53	15.19	176.82
21	6	375	4.15	4.81	3.61	16.87	179.39
22	6	375	4.40	4.87	3.64	17.22	176.58
23	6	375	4.65	4.68	3.37	16.91	175.24
24	6	375	4.90	4.56	3.39	15.93	174.03
25	6	400	4.15	4.31	3.57	17.77	178.68
26	6	400	4.40	4.97	3.91	17.26	177.26
27	6	400	4.65	4.75	3.55	16.86	174.71
28	6	400	4.90	4.41	3.45	15.48	170.66
29	6	425	4.15	4.79	3.80	16.78	171.47
30	6	425	4.40	4.84	4.06	16.96	172.38
31	6	425	4.65	4.70	3.63	16.87	169.56
32	6	425	4.90	4.62	3.76	17.06	166.78
33	7	350	4.15	6.04	4.36	22.56	162.54
34	7	350	4.40	5.85	3.98	23.22	161.93
35	7	350	4.65	5.86	3.91	22.30	158.29
36	7	350	4.90	5.83	3.86	22.08	159.44
37	7	375	4.15	6.31	3.70	23.72	158.74
38	7	375	4.40	6.05	3.63	23.29	154.99
39	7	375	4.65	6.25	4.02	23.96	154.36
40	7	375	4.90	5.66	4.04	22.49	153.78
41	7	400	4.15	6.17	3.44	24.02	155.45
42	7	400	4.40	6.37	3.97	23.58	154.80
43	7	400	4.65	5.67	3.97	22.66	154.06
44	7	400	4.90	5.65	3.61	23.65	152.16
45	7	425	4.15	6.14	4.46	23.12	155.49
46	7	425	4.40	5.76	4.24	22.55	153.55
47	7	425	4.65	5.48	4.16	23.21	150.70
48	7	425	4.90	6.14	4.09	22.72	149.46
49	8	350	4.15	7.18	4.23	25.54	145.46
50	8	350	4.40	6.88	4.92	23.12	143.57
51	8	350	4.65	6.97	4.40	23.26	143.29
52	8	350	4.90	7.13	4.47	23.80	139.57
53	8	375	4.15	6.92	4.20	24.18	139.55
54	8	375	4.40	7.23	4.52	24.10	139.98
55	8	375	4.65	7.14	4.68	24.12	139.82
56	8	375	4.90	7.06	4.24	23.85	137.13
57	8	400	4.15	6.73	4.24	24.07	140.08
58	8	400	4.40	7.20	4.06	23.78	139.10
59	8	400	4.65	7.10	4.11	24.63	137.08
60	8	400	4.90	7.23	3.90	24.92	137.95

Table 14   continued

Sl. No.	Welding parameters			Output parameters			
	WC, kA	WT, ms	EF, kN	ND, mm	PS, kN	TSS, kN	MDCR, $\mu\Omega$
61	8	425	4.15	6.81	3.95	24.24	137.27
62	8	425	4.40	7.11	4.14	24.67	136.23
63	8	425	4.65	7.10	3.71	24.57	133.57
64	8	425	4.90	7.05	4.01	24.29	130.90

References

1. P. Podržaj, I. Polajnar, J. Diaci, and Z. Kariž, Overview of Resistance Spot Welding Control, *Sci. Technol. Welding Joining*, 2008, **13**(3), p 215–224

2. N.T. Williams and J.D. Parker, Review of Resistance Spot Welding of Steel Sheets: Part 1 - Modelling and Control of Weld Nugget Formation, *Int. Mater. Rev.*, 2004, **49**, p 45–75

3. M. Pouranvari and S.P.H. Marashi, Critical Review of Automotive Steels Spot Welding: Process, Structure and Properties, *Sci. Technol. Welding Joining*, 2013, **18**(5), p 361–403

4. J.P. Oliveira, K. Ponder, E. Brizes, T. Abke, P. Edwards, and A.J. Ramirez, Combining Resistance Spot Welding and Friction Element Welding for Dissimilar Joining of Aluminum to High Strength Steels, *J. Mater. Process. Technol.*, 2019, **273**, p 116192. https://doi.org/10.1016/j.jmatprotec.2019.04.018

5. D. Zhao, Y. Wang, D. Liang, and P. Zhang, Modeling and Process Analysis of Resistance Spot Welded DP600 Joints Based on Regression Analysis, *Mater. Des.*, 2016, **110**, p 676–684

6. M. Pouranvari, Critical Assessment: Dissimilar Resistance Spot Welding of Aluminium/Steel: Challenges and Opportunities, *Mater. Sci. Technol.*, 2017, **33**(15), p 1705–1712

7. K. Zhou and P. Yao, Review of Application of the Electrical Structure in Resistance Spot Welding, *IEEE Access*, 2017, **5**, p 25741–25749

8. B. Asati, N. Shajan, V.T. Akhil Kishore, K.S. Arora, and R.G. Narayanan, A Comparative Investigation on Self-Piercing Riveting and Resistance Spot Welding of Automotive Grade Dissimilar Galvanized Steel Sheets, *Int. J. Adv. Manuf. Technol.*, 2022, **123**(3–4), p 1079–1097

9. A.K. Vt, B. Asati, N. Shajan, and K.S. Arora, Performance Evaluation of Self-Piercing Riveted and Resistance Spot Welded Dissimilar Steel Joints, *ARAI J. Mob. Technol.*, 2021, **1**(1), p 34–42

10. A.M. Al-Mukhtar, Review of Resistance Spot Welding Sheets: Processes and Failure Mode, *Adv. Eng. Forum*, 2016, **17**, p 31–57

11. B. Asati, R.G. Narayanan, N. Shajan, and K.S. Arora, Effect of Die Design and Sheet Placement on Self- Piercing Rivet of Automotive Steels and Comparison with Resistance Spot and Friction Stir Spot Welding, *J. Mater. Eng. Perform.*, 2022 https://doi.org/10.1007/s11665-022-07762-9

12. S.M. Manladan, F. Yusof, S. Ramesh, Y. Zhang, Z. Luo, and Z. Ling, Microstructure and Mechanical Properties of Resistance Spot Welded in Welding-Brazing Mode and Resistance Element Welded Magnesium Alloy/Austenitic Stainless Steel Joints, *J. Mater. Process. Technol.*, 2017, **250**, p 45–54

13. M. Hamedi and M. Atashparva, A Review of Electrical Contact Resistance Modeling in Resistance Spot Welding, *Welding World*, 2017, **61**(2), p 269–290

14. S. Thapliyal and A. Mishra, Machine Learning Classification-Based Approach for Mechanical Properties of Friction Stir Welding of Copper, *Manuf. Lett.*, 2021, **29**, p 52–55

15. I. Baturynska, O. Semeniuta, and K. Martinsen, Optimization of Process Parameters for Powder Bed Fusion Additive Manufacturing by Combination of Machine Learning and Finite Element Method: A ConceptualFramework, *Proc. CIRP*, 2018, **67**, p 227–232. https://doi.org/10.1016/j.procir.2017.12.204

16. P.C. Collins and D.G. Harlow, Probability and Statistical Modeling: Ti-6Al-4V Produced via Directed Energy Deposition, *J. Mater. Eng. Perform.*, 2021, **30**(9), p 6905–6912. https://doi.org/10.1007/s11665-021-06062-y

17. K.L. Raju, S. Thapliyal, S. Sigatapu, A.K. Shukla, G. Bajargan, and B. Pant, Process Parameter Dependent Machine Learning Model for Densification Prediction of Selective Laser Melted Al-50Si Alloy and Its Validation, *J. Mater. Eng. Perform.*, 2022, **31**(10), p 8451–8458. https://doi.org/10.1007/s11665-022-06831-3

18. T. Nasir, M. Asmaela, Q. Zeeshana, and D. Solyalib, Applications of Machine Learning to Friction Stir Welding Process Optimization, *J. Kejuruteraan*, 2020, **32**(1), p 171–186

19. B. Zhou, T. Pychynski, M. Reischl, E. Kharlamov, and R. Mikut, Machine Learning with Domain Knowledge for Predictive Quality Monitoring in Resistance Spot Welding, *J. Intell. Manuf.*, 2022, **33**(4), p 1139–1163

20. S.M. Ali, N.N. Johnson, V. Madhavadas, A. Giri, J. Sahu, S.P. Anand, and C.S. Srivas, Investigation on the Effect of Grinding Wheel for Grinding of AISI D3 Tool Steel under Different Conditions, *Eng. Res. Express*, 2022, **4**(4), p 045036. https://doi.org/10.1088/2631-8695/aca956

21. R. Mamedipaka and S. Thapliyal, Data-Driven Model for Predicting Tensile Properties of Wire Arc Additive Manufactured 316L Steels and Its Validation, *J. Mater. Eng. Perform.*, 2023 https://doi.org/10.1007/s11665-023-08071-5

22. K. Nomura, K. Fukushima, T. Matsumura, and S. Asai, Burn-through Prediction and Weld Depth Estimation by Deep Learning Model Monitoring the Molten Pool in Gas Metal Arc Welding with Gap Fluctuation, *J. Manuf. Process.*, 2021, **61**, p 590–600

23. A. Mayr, D. Kißkalt, M. Meiners, B. Lutz, F. Schäfer, R. Seidel, A. Selmaier, J. Fuchs, M. Metzner, A. Blank, and J. Franke, Machine Learning in Production - Potentials, Challenges and Exemplary Applications, *Proc. CIRP*, 2020, **86**, p 49–54

24. M.A. Kesse, E. Buah, H. Handroos, and G.K. Ayetor, Development of an Artificial Intelligence Powered Tig Welding Algorithm for the Prediction of Bead Geometry for Tig Welding Processes Using Hybrid Deep Learning, *Metals (Basel)*, 2020, **10**(4), p 451

25. H. Kitano, A. Sato, M. Iyota, and T. Nakamura, Investigation of Relationship between Resistance Spot Welding Condition and Nugget Shape by Utilizing Machine Learning Based Technique, *Welding Int.*, 2019, **33**(4–6), p 223–230

26. R. Sizyakin, V. Voronin, N. Gapon, A. Zelensky, and A. Pižurica, Automatic Detection of Welding Defects Using the Convolutional Neural Network, *Proc. SPIE*, 2019 https://doi.org/10.1117/12.2525643

27. J. Shen, R. Gonçalves, Y.T. Choi, J.G. Lopes, J. Yang, N. Schell, H.S. Kim, and J.P. Oliveira, Microstructure and Mechanical Properties of Gas Metal Arc Welded CoCrFeMnNi Joints Using a 410 Stainless Steel Filler Metal, *Mater. Sci. Eng. A*, 2022, **857**, p 144025. https://doi.org/10.1016/j.msea.2022.144025

28. J. Shen, P. Agrawal, T.A. Rodrigues, J.G. Lopes, N. Schell, Z. Zeng, R.S. Mishra, and J.P. Oliveira, Gas Tungsten Arc Welding of As-Cast AlCoCrFeNi$_{2.1}$ Eutectic High Entropy Alloy, *Mater. Des.*, 2022, **223**, p 111176. https://doi.org/10.1016/j.matdes.2022.111176

29. J. Shen, R. Gonçalves, Y.T. Choi, J.G. Lopes, J. Yang, N. Schell, H.S. Kim, and J.P. Oliveira, Microstructure and Mechanical Properties of Gas Metal Arc Welded CoCrFeMnNi Joints Using a 308 Stainless Steel Filler Metal, *Scr. Mater.*, 2023, **222**, p 115053. https://doi.org/10.1016/j.scriptamat.2022.115053

30. A. Sumesh, K. Rameshkumar, K. Mohandas, and R.S. Babu, Use of Machine Learning Algorithms for Weld Quality Monitoring Using Acoustic Signature, *Proc. Comput. Sci.*, 2015, **50**, p 316–322

31. H. Wang, D. He, M. Liao, P. Liu, and R. Lai, Study on Quality Prediction of 2219 Aluminum Alloy Friction Stir Welding Based on Real-Time Temperature Signal, *Materials*, 2021, **14**(13), p 3496

32. P. Rodríguez-Gonzálvez and M. Rodríguez-Martín, Weld Bead Detection Based on 3D Geometric Features and Machine Learning Approaches, *IEEE Access*, 2019, **7**, p 14714–14727

33. I. Hwang, H. Yun, J. Yoon, M. Kang, D. Kim, and Y.M. Kim, Prediction of Resistance Spot Weld Quality of 780 MPa Grade Steel

Using Adaptive Resonance Theory Artificial Neural Networks, *Metals (Basel)*, 2018, **8**(6), p 453

34. S. Li, L. Zhang, H. Zhao, L. Qi, and Y. Kang, Mechanical Behavior of DP780 Dual Phase Steel at a Wide Range of Strain Rates, *Mater. Res. Express*, 2018, **5**(9), p 096519

35. S.-C. Han, U.M. Chaudry, J.-Y. Yoon, and T.-S. Jun, Investigating Local Strain Rate Sensitivity of the Individual Weld Zone in the Friction Stir Welded DP 780 Steel, *J. Market. Res.*, 2022, **20**, p 508–515. https://doi.org/10.1016/j.jmrt.2022.07.125

36. E. Sariev and G. Germano, Bayesian Regularized Artificial Neural Networks for the Estimation of the Probability of Default, *Quant Finance*, 2020, **20**(2), p 311–328. https://doi.org/10.1080/14697688.2019.1633014

37. S. Sanaye and H. Hajabdollahi, Thermal-Economic Multi-Objective Optimization of Plate Fin Heat Exchanger Using Genetic Algorithm, *Appl. Energy Ltd*, 2010, **87**(6), p 1893–1902

38. A. Konak, D.W. Coit, and A.E. Smith, Multi-Objective Optimization Using Genetic Algorithms: A Tutorial, *Reliab. Eng. Syst. Saf.*, 2006, **91**(9), p 992–1007

39. M. Pouranvari, H.R. Asgari, S.M. Mosavizadch, P.H. Marashi, and M. Goodarzi, Effect of Weld Nugget Size on Overload Failure Mode of Resistance Spot Welds, *Sci. Technol. Weld. Joining*, 2007, **12**(3), p 217–225

40. M. Sheikhi, S. Jaderian, Y. Mazaheri, and M. Pouranvari, Prediction of the Failure Mode of Automotive Steels Resistance Spot Welds, *Sci. Technol. Welding Joining*, 2020, **25**(6), p 511–517

41. S.S. Rao, K.S. Arora, L. Sharma, and R. Chhibber, Investigations on Mechanical Behaviour and Failure Mechanism of Resistance Spot-Welded DP590 Steel Using Artificial Neural Network, *Trans. Indian Inst. Metals*, 2021, **74**(6), p 1419–1438

42. A.M. Pereira, J.M. Ferreira, A. Loureiro, J.D.M. Costa, and P.J. Bártolo, Effect of Process Parameters on the Strength of Resistance Spot Welds in 6082–T6 Aluminium Alloy, *Mater. Des.*, 2010, **31**(5), p 2454–2463

43. Y. Luo, W. Rui, X. Xie, and Y. Zhu, Study on the Nugget Growth in Single-Phase AC Resistance Spot Welding Based on the Calculation of Dynamic Resistance, *J. Mater. Process. Technol.*, 2016, **229**, p 492–500

44. H. Pashazadeh, Y. Gheisari, and M. Hamedi, Statistical Modeling and Optimization of Resistance Spot Welding Process Parameters Using Neural Networks and Multi-Objective Genetic Algorithm, *J. Intell. Manuf.*, 2016, **27**(3), p 549–559

45. D.W. Zhao, Y.X. Wang, L. Zhang, and P. Zhang, Effects of Electrode Force on Microstructure and Mechanical Behavior of the Resistance Spot Welded DP600 Joint, *Mater. Des.*, 2013, **50**, p 72–77

46. C. Rajarajan, P. Sivaraj, M. Seeman, and V. Balasubramanian, Influence of Electrode Force on Metallurgical Studies and Mechanical Properties of Resistance Spot Welded Dual Phase (DP800) Steel Joints, *Mater. Today Proc.*, 2020, **22**, p 614–618

47. F. Chen, Y. Wang, S. Sun, Z. Ma, and X. Huang, Multi-Objective Optimization of Mechanical Quality and Stability during Micro Resistance Spot Welding, *Int. J. Adv. Manuf. Technol.*, 2019, **101**(5–8), p 1903–1913

48. H. Moshayedi and I. Sattari-Far, Numerical and Experimental Study of Nugget Size Growth in Resistance Spot Welding of Austenitic Stainless Steels, *J. Mater. Process. Technol.*, 2012, **212**(2), p 347–354. https://doi.org/10.1016/j.jmatprotec.2011.09.004

49. H. Eisazadeh, M. Hamedi, and A. Halvaee, New Parametric Study of Nugget Size in Resistance Spot Welding Process Using Finite Element Method, *Mater. Des.*, 2010, **31**(1), p 149–157

50. Z. Zhang, X. Yang, J. Zhang, G. Zhou, X. Xu, and B. Zou, Effect of Welding Parameters on Microstructure and Mechanical Properties of Friction Stir Spot Welded 5052 Aluminum Alloy, *Mater. Des.*, 2011, **32**(8–9), p 4461–4470

51. M. Pouranvari, Susceptibility to Interfacial Failure Mode in Similar and Dissimilar Resistance Spot Welds of DP600 Dual Phase Steel and Low Carbon Steel during Cross-Tension and Tensile-Shear Loading Conditions, *Mater. Sci. Eng., A*, 2012, **546**, p 129–138

52. M. Pouranvari and P. Marashi, Failure Behaviour of Resistance Spot Welded Low Carbon Steel in Tensile-Shear and Coach-Peel Tests: A Comparative Study, *Metall. J. Metall.*, 2009, **15**(3), p 149–157

53. F. Hayat and I. Sevim, The Effect of Welding Parameters on Fracture Toughness of Resistance Spot- Welded Galvanized DP600 Automotive Steel Sheets, *Int. J. Adv. Manuf. Technol.*, 2012, **58**(9–12), p 1043–1050

54. K. Zhou and L. Cai, Online Nugget Diameter Control System for Resistance Spot Welding, *Int. J. Adv. Manuf. Technol.*, 2013, **68**(9–12), p 2571–2588

55. M.W. Dewan, D.J. Huggett, T. Warren Liao, M.A. Wahab, and A.M. Okeil, Prediction of Tensile Strength of Friction Stir Weld Joints with Adaptive Neuro-Fuzzy Inference System (ANFIS) and Neural Network, *Mater Des*, 2016, **92**, p 288–299

56. M.F.A. Zaharuddin, D. Kim, and S. Rhee, An ANFIS Based Approach for Predicting the Weld Strength of Resistance Spot Welding in Artificial Intelligence Development, *J. Mech. Sci. Technol.*, 2017, **31**(11), p 5467–5476

57. B.V. Feujofack Kemda, N. Barka, M. Jahazi, and D. Osmani, Multi-Objective Optimization of Process Parameters in Resistance Spot Welding of A36 Mild Steel and Hot Dipped Galvanized Steel Sheets Using Non-Dominated Sorting Genetic Algorithm, *Metals Mater. Int.*, 2022, **28**(2), p 487–502

58. X. Wan, Y. Wang, and D. Zhao, Multi-Response Optimization in Small Scale Resistance Spot Welding of Titanium Alloy by Principal Component Analysis and Genetic Algorithm, *Int. J. Adv. Manuf. Technol.*, 2016, **83**(1–4), p 545–559

59. L. Boriwal, M.M. Mahapatra, and P. Biswas, Modelling and Optimizing the Effects of Process Parameters on Galvanized Steel Sheet Resistance Spot Welds, *Proc. Inst. Mech. Eng. Part B J. Eng. Manuf.*, 2012, **226**(4), p 664–674

60. S.S. Rao, K.S. Arora, L. Sharma, and R. Chhibber, Modelling and Optimization of Resistance Spot Weld Responses Using RSM–GA Technique for DP590 Steel Sheets, *Proc. Natl. Acad. Sci. India Sect. A Phys. Sci.*, 2022, **92**(3), p 453–466